The Journal of Undergraduate Research in Physics

CONTENTS

Volume 19, Number 1
Fall, 2000

Produced by the Physics Department of Guilford College
for
The American Institute of Physics and the Society of Physics Students

THE JOURNAL OF UNDERGRADUATE RESEARCH IN PHYSICS

This journal is devoted to research work done by undergraduate students in physics and its related fields. It is a vehicle for the exchange of ideas and information by undergraduate students. Information for students wishing to submit manuscripts for possible inclusion in the Journal follows.

ELIGIBILITY
The author(s) must have performed all work reported in the paper as an undergraduate student(s). The subject matter of the paper is open to any area of pure or applied physics or physics related field.

SPONSORSHIP
Each paper must be sponsored by a full-time faculty member of the department in which the research was done. A letter from the sponsor, certifying that the work was done by the author as an undergraduate and that the sponsor is willing to be acknowledged at the end of the paper, must accompany the manuscript if it is to be considered for publication.

SUBMISSION
Two copies of the manuscript, the letter from the sponsor and a telephone number or E-Mail address where the author can be reached should be sent to:
Dr. Rexford E. Adelberger, Editor
THE JOURNAL OF UNDERGRADUATE RESEARCH IN PHYSICS
Physics Department
Guilford College
Greensboro, NC 27410

FORM
The manuscript should be typed, double spaced, on 8 1/2 x 11 inch sheets. Margins of about 1.5 inches should be left on the top, sides, and bottom of each page. Papers should be limited to fifteen pages of text in addition to an abstract (not to exceed 250 words) and appropriate drawings, pictures, and tables. Manuscripts may be submitted on a disk or as an E-mail attachment that can be read by a MacIntosh™. The files must be compatible with MicroSoft Word™ or PageMaker™.

ILLUSTRATIONS
Line drawings should be made with black ink on plain white paper. The line thickness should be sufficient to be reduced to column format. Each figure or table must be on a separate sheet. Photographs must have a high gloss finish. If the submission is on a disk, the illustrations should be in PICT, TIFF or EPS format.

CAPTIONS
A descriptive caption should be provided for each illustration or table, but it should not be part of the figure. The captions should be listed together at the end of the manuscript

EQUATIONS
Equations should appear on separate lines, and may be written in black ink. All equations should be numbered. We use EXPRESSIONIST™ to format equations in the Journal.

FOOTNOTES
Footnotes should be typed, double spaced and grouped together in sequence at the end of the manuscript.

PREPARING A MANUSCRIPT
A more detailed set of instructions and advice for authors wishing to prepare manuscripts for publication in the Journal of Undergraduate Research in Physics can be found in the back of each issue.

SUBSCRIPTION INFORMATION

The Journal is published twice each academic year, issue # 1 appearing in the fall and issue # 2 in the spring of the next calendar year. There are two issues per volume.

TYPE OF SUBSCRIBER	PRICE PER VOLUME
Individual	$US 5.00
Institution	$US 10.00

Foreign subscribers add $US 2.00 for surface postage, $US 10.00 for air freight.

Back issues may be purchased by sending $US 15.00 per volume to the editorial office.

To receive a subscription, send your name, address, and check made out to **The Journal of Undergraduate Research in Physics (JURP)** to the editorial office:

JURP
Physics Department
Guilford College
Greensboro, NC 27410

The Journal of Undergraduate Research in Physics is sent to each member of the Society of Physics Students as part of their annual dues.

VOLUME 19

ACADEMIC YEAR 2000-2001

The Journal of Undergraduate Research in Physics

Produced by the Physics Department
of Guilford College
for
The American Institute of Physics
and
The Society of Physics Students

ISSN 0731 - 3764

ANOMALOUS DIFFUSION AND THE EGG CRATE POTENTIAL: A NUMERICAL STUDY IN CHAOTIC HAMILTONIAN DYNAMICS

M. Golladay †
Physics Department
Roanoke College, Salem, VA 24153

ABSTRACT

The motion of a classical particle in an "egg-crate" potential is modeled in an effort to understand chaotic Hamiltonian dynamics. While all energy levels are examined, our main interests are in energies that are associated with anomalous diffusion. However, periodic motion and classical Brownian motion are observed at various energy levels in the system. It is noted in particular that particles with energies between the saddle point of the potential and below the absolute maximum exhibit anomalous diffusion. The power spectra at these levels exhibit $1/f$ noise. Algebraic tails are present in the velocity autocorrelation functions of the energies with $1/f$ noise. Further exploration of these tails suggests that multiple types are present at different energies.

INTRODUCTION

The study of chaotic dynamics and Lévy walks is a relatively new branch of dynamic systems theory. Its roots, however, are buried in the development of theories on Brownian motion, which was first reported in 1785 by Jan Ingenhausz, a Dutch physicist [1]. The phenomenon, generally associated with the motion of particles in fluids, was named after Robert Brown due to his work in the field in the nineteenth century, although many physicists, including Albert Einstein, have also examined it. For our purposes, it suffices to classify Brownian motion as 'classical diffusive motion,' characterized by the property that the root-mean-square deviation of the position grows linearly with time. While this classical diffusion is observed in our system, it is not our main focus. In general, diffusive motion demonstrates the following relationship:

$$< r^2 > \approx t^{\gamma} \qquad (1)$$

where r is position and t is time. When $\gamma = 1$, the diffusion is classical. However, for all other values of γ, the diffusion is anomalous. When $\gamma < 1$, it is called 'subdiffusion', and $\gamma > 1$ is called 'superdiffusion'.

With the advent of increasingly powerful computers and computational methods, the movement toward numerically studying previously unsolvable systems is a natural one. Recently, the study of systems involving fairly complex and nonlinear partial differential equations has become a rich field. However, due to the approximate nature of numerical methods, it is often easy to mistake a numerical error or property for a physical property of the system one is studying. This makes it necessary to verify the results of any numerical model so that one can be sure that any 'abnormal' or surprising results are in truth related to the system itself and not to the numerical method used to solve it.

With this in mind, we return to the discussion of the types of different diffusive motion. As recently as twenty years ago, the first examples of enhanced diffusion related to random walks were discovered [3]. Christened 'Lévy walks', these random walks have as their chief characteristic a pattern of self-similar jumps. Thus, rather than exhibiting classical diffusion, Lévy walks demonstrate motion that is 'beyond Brownian' [1]. The nomenclature 'Lévy walk' was chosen due to the similarity of the jumps in these cases of enhanced diffusion to the steps in the well-known Lévy flights; the average jump length is infinite in individual steps [3].

Molly is currently a graduate student with the physics department at Cornell University. This research was begun during the summer before her senior year at Roanoke College through their undergraduate research program. When she isn't studying nonlinear dynamics, Molly is often seen playing her violin or volunteering at the local SPCA.

In this work, we examine a specific example of a Lévy walk, associated with the motion of a classical particle in the egg-crate potential, in verification of work done previously by T. Geisel *et al.* [3]. We provide a detailed description of the system and its solution at different energy levels. We then examine the energy levels that exhibit classical diffusion and deal with the energy levels that exhibit anomalous diffusion.

THE EGG-CRATE POTENTIAL

Figure 1 is a graphical representation of the "egg-crate" potential, so named due to its periodic shape bearing a resemblance to an egg-crate. It should be noted that the minima exist at $V = 0$, the maxima at $V = 6$, and saddle points where $V = 2$. Essentially, the potential can be viewed as a group of "cells," each of width and length 2π. These physical characteristics of the potential play a role in the behavior of the test particle at certain energy levels.

$$V(x,y) = V(\vec{r}) = \sum V_g e^{i\vec{g}\cdot\vec{r}}. \quad (2)$$

We chose to use a two-dimensional Fourier series representation of this nonlinear 'egg-crate' potential of the form:

For simplicity, we used the first three terms of this series to represent our potential:

$$V(x,y) = a + b\left[\cos(x) + \cos(y)\right] + c\left[\cos(x)\cos(y)\right]. \quad (3)$$

where $a = 2.5$, $b = 1.5$, and $c = 0.5$. The units have been non-dimensionalized throughout this paper to facilitate the numerical nature of our work.

The motion of a test particle of mass unity in the system is simulated using its Hamiltonian:

$$H = \frac{v_x^2}{2} + \frac{v_y^2}{2} + V(x,y). \quad (4)$$

However, to apply the necessary method for numerical solution, the Hamiltonian equations of motion had to be applied to determine the acceleration in each direction.

$$a_x = -\sin(x)\left[b + c\cos(y)\right]$$
$$a_y = -\sin(y)\left[b + c\cos(x)\right]. \quad (5)$$

Equation 5 represent two first-order differential equations whose solutions are v_x and v_y respectively. When combined with the fact that velocity is itself the first order time derivative of position, two systems of two first-order ODE's, one for the x-coordinate, the other for the y-coordinate, resulted. Acceleration and velocity were then solved for to determine the velocity and position, respectively. The 4th order Rungé-Kutta method was used to integrate the system of equations.

It must be emphasized here that by using numerical techniques to solve and analyze the motion in this potential, error is inevitably introduced into any solution. It is this fact that makes the previous findings [2,3] subject to further analysis. The error due to the numerical approximations must at all times be monitored carefully so that one can be assured that all behaviors observed in the system originate from the system and not from the numerics themselves. First and foremost, due to the Hamiltonian nature of this system, energy must be conserved at all times. To monitor this, we used the relationship between the variance of the total energy with respect to our variables (x, y, v_x, v_y, and t):

$$\sigma_E^2 = \sigma_x^2\frac{\partial^2 H}{\partial x^2} + \sigma_y^2\frac{\partial^2 H}{\partial y^2} + \sigma_{v_x}^2\frac{\partial^2 H}{\partial v_x^2} + \sigma_{v_y}^2\frac{\partial^2 H}{\partial v_y^2}, \quad (6)$$

where

$$\sigma_x^2 = \sigma_x^2 = \sigma_{v_x}^2 = \sigma_{v_x}^2 = (dt)^2, \quad (7)$$

and dt is the step size. The variance of the energy, then, depends on step size and initial conditions. This is monitored through calculating σ_E within the simulation by computing the particle's total energy at various points during execution. If σ_E is within our established bound, as shown below, the energy is conserved and the numerical error is within acceptable limits.

For this experiment, we chose an initial value of $x = -10$ and an initial for $y = 5$. Solving the variance equation (Equation 6), shows that $\sigma_E^2 \leq 3.071\ (dt^2)$. We chose $(dt) = 10^{-2}$, implying that $\sigma_E \leq 1.75\text{x}10^{-2}$ and calculated σ_E within the simulation consistently to be $\approx 10^{-8}$. Thus, the numerical error due to our simulation is within acceptable bounds.

The solution to our system of ODE's yielded different results at different energy levels, but a definite relationship between behaviors at certain levels emerged:

$E < 2.0$	periodic motion
$2.0 < E < 4.6$	anomalous diffusion
$5.0 < E < 6.0$	classical diffusion
$E > 6.0$	'free' particle motion

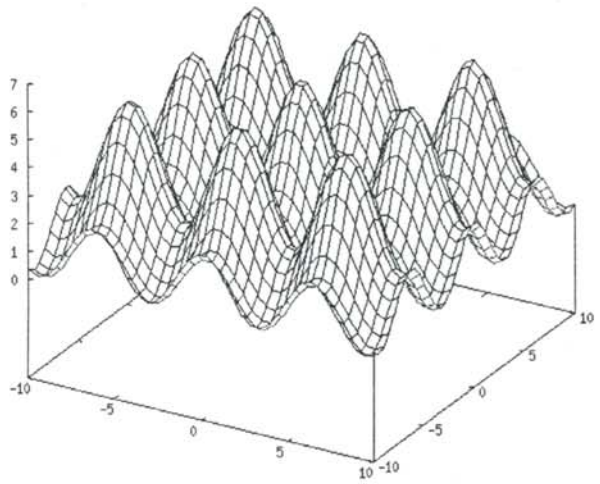

Figure 1
The periodic, nonlinear egg-crate potential $V(x,y) = a + b[\cos(x) + \cos(y)] + c\,[\cos(x)\cos(y)]$, where $a = 2.5$, $b = 1.5$, and $c = 0.5$.

The particle trajectories for these energy levels are shown in Figure 2 [4]. It should be noted that upon examination of the trajectories only, one cannot distinguish between the anomalous diffusion levels and the classical diffusion levels. A more detailed examination of the behavior at each energy level is required.

The motion of our test particle depends primarily on two characteristics: the initial energy of the particle; and secondly, the initial position of the particle. To focus entirely on the particle's energy and its effect on the particle's behavior, we have held the initial position of the particle constant at all energy levels: $x = -10$ and $y = 5$. This places the particle completely inside of a single cell in the potential.

As the behavior of the system at various energies was examined, a definite structure of energy levels became apparent. The behavior at each group of energy levels will be discussed separately, starting with the most 'trivial' case.

For all energies above $E = 6$, the particle's energy exceeds the maximum energy of the potential. Thus, the particle is considered 'free', able to follow a trajectory not confined by the potential. At these energies, the particle does not interact in a complex fashion with the potential and, therefore, is not very interesting to study in connection with this potential. It should be noted that for energies greater than but fairly close to $E = 6$, the particle still feels the effects of the potential, but its motion is not confined to the anatomy of the potential itself, thus eliminating the complex behavior observed in lower energies.

Particles with energies $E < 2$ undergo periodic motion,

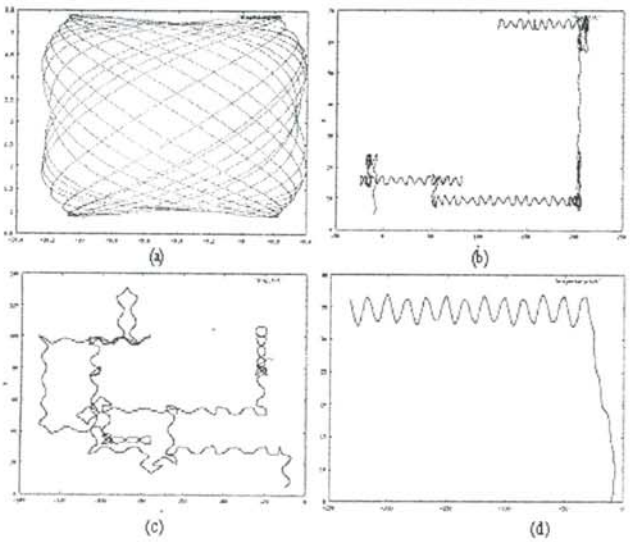

Figure 2

Trajectory of particle at energies (a) E=2. (b) E=4. (c) E=5.5 (d) E=6.0. The horizontal axis is the x position and the vertical axis is the y position of the particle at a given time.

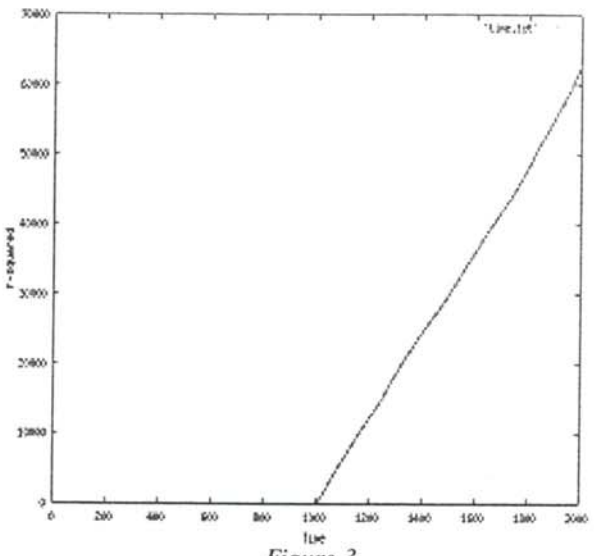

Figure 3

Time series (<r²> vs time) for energy E = 5.5. The linear relationship between t and <r²> indicates classical diffusion.

'trapped' in a single cell. It is possible to determine the period of this motion, but it depends strongly on the initial conditions of the particle and requires solution of the quadrature:

$$T = 2\iint \frac{1}{\sqrt{2[E - V(x,y)]}} dy\, dx, \tag{8}$$

where the limits of integration are the turning points of the particle and are not trivial to locate. Thus, if the initial conditions vary even slightly, the turning points are altered and thus, the period is changed.

For more interesting behaviors, then, we turn to energies between the saddle points and the absolute maxima. The following sections will discuss the diffusive behavior observed at these energy levels in detail.

CLASSICAL DIFFUSION

It has been previously suggested [3] that one can determine two distinct types of diffusion for energies between $E = 2$ and $E = 6$. So we began looking at each 'set' of energies discretely in an attempt to validate these findings. In the upper energies (those between $E = 5$ and $E = 6$), we expected to find classical Brownian motion.

The main characteristic of classical Brownian motion is the following relationship:

$$< x^2 > = (2D)\, t, \tag{9}$$

where D is the diffusion coefficient. Therefore, this relationship should hold true for $5 < E < 6$. However, since our system is two-dimensional, Equation 9 must be adapted to suit our needs:

$$< r^2 > = (4D)\, t, \tag{10}$$

where $r^2 = x^2 + y^2$. We created a time series graph where we plotted time versus r^2. Figure 3 depicts our findings.

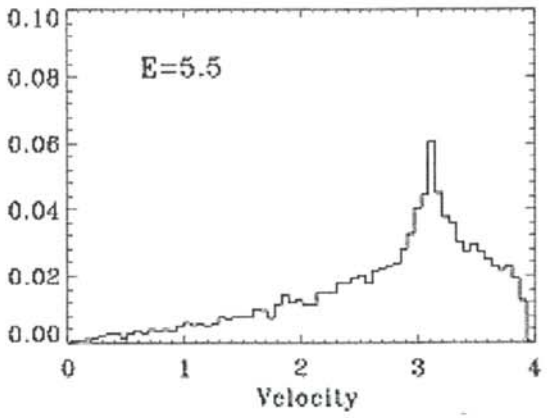

Figure 4
The velocity distribution function for energy E = 5.5. The chi-squared structure here is consistent with each of the velocity components being a normally distributed random variable, i.e., classical diffusion.

The right-hand side of Figure 3 shows the time series for $E = 5.5$, demonstrating the linear relationship between r^2 and t. The diffusion coefficient for this energy level can then be found from the slope of the line.

We also have used a binning technique to examine the distribution of the velocity values during a simulation. This technique has revealed a chi-squared distribution, implying that the velocity components are normally distributed random variables, suggesting classical diffusion. Figure 4 shows one such distribution for $E = 5.5$.

We used a third technique, the Poincar surface-of-section, to support our claim that for energies between $E = 5$ and $E = 6$, classical diffusive motion is observed. The purpose of this technique is to reduce an unwieldy four-dimensional phase space to a two-dimensional representation through taking a series of 'cuts' in this space. Our cut was in essence a 'recording' of every time the particle changed cells (the cell boundaries occur when $x = 2\pi n$, where n is an integer. When the particle has crossed this line, the y-coordinate and the v_y-coordinate (mod 2π) are recorded. This record constitutes the Poincaré sections. Figure 5 shows the surface-of-section for $E = 5.5$. The apparent non-deterministic behavior suggests diffusion, but one that has no fractal structure, such as in classical diffusion. Figure 5 is important only as a foil to the surface-of-section diagrams for anomalously diffusing particles.

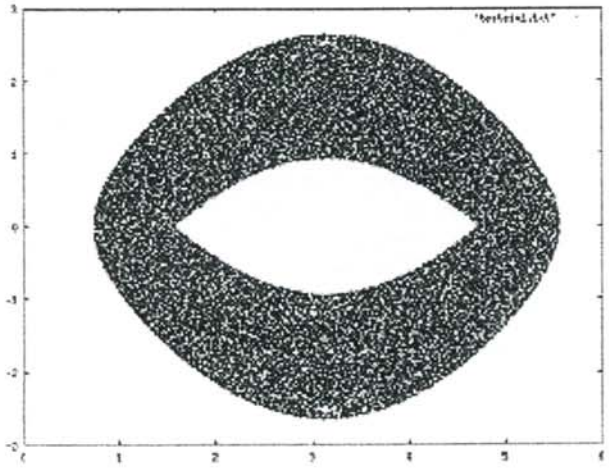

Figure 5
Poincaré surface-of-section (y vs v_y) for energy E=5.5 at the cell boundaries $x = 2\pi n$. It should be noted that the lack of a fractal structure implies the classical nature of the diffusion.

Anomalous Diffusion

And so, we have the hypothesis [3] that energies between $E = 5$ and $E = 6$ exhibit classical diffusion, leading us to examine the conjecture that the energy levels beneath this display non-classical diffusive behavior.

Our first tool here is the Poincaré surface-of-section. Two sections are shown graphically in Figure 5 ($E = 5.5$) and Figure 6 ($E = 4.0$). The former is an example of classical diffusion. It is important to compare Figure 5 to Figure 6 to understand the distinction between the two types of

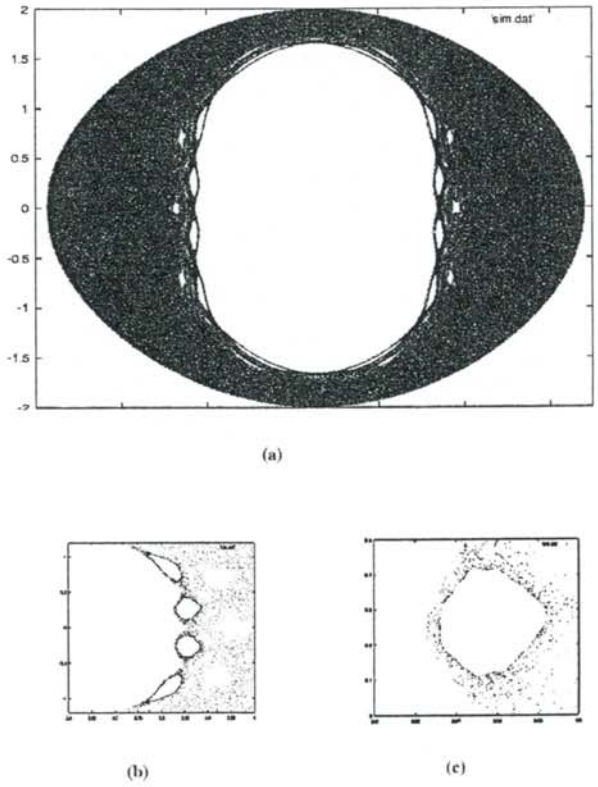

Figure 6
(a) Poincaré surface-of-section for energy E = 4 at the cell boundaries ($x = 2\pi n$). (b) and (c) are magnifications of the same plot, emphasizing the self-replicating, or fractal, structure exhibited in the daughter islands.

diffusion. Figure 6 is more structured than Figure 5, indicating that a more complex behavior is occurring in the particle's motion. Also, Figure 5 demonstrates the self-similar structure that is a hallmark of chaotic systems, as well as the characteristic cantori, or island, structure. The surface-of-section implies diffusive behavior, but hints at a more complex chaotic motion than observed previously in the higher energy levels.

To examine this further, the same time series technique is applied to this 'set' of lower energies that was discussed in the previous section. This is done to establish a more clear picture of this anomalous behavior in terms of the definition of diffusive motion as described in Equation 1. In short, we desire to obtain an estimate for the parameter γ that defines the nature of the diffusion. Figure 7 shows our results for $E = 4.0$ and indicates that for energies between $E = 2$ and $E = 4.6$, γ is greater than 1, establishing a superdiffusive motion in these energies.

Now that the superdiffusive nature of the particle's motion has been established, we turn to statistical analysis to gain insight into the motion itself. First, we examine the velocity distribution function of the system. Figure 8, using the same binning technique mentioned previously, shows the distribution function for the velocities at $E = 4.6$. The distribution suggests that the velocity components are not normally distributed random variables, indicating interesting statistical behavior at these energies. This is to be expected given the strange nature of the diffusion.

We now examine the velocity autocorrelation function of the system. The autocorrelation function in essence is a graphical representation of the "memory" of the particle, described by the following relation [6]:

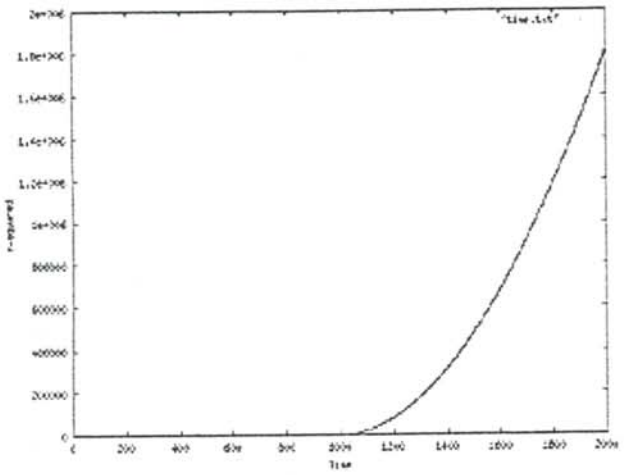

Figure 7
Time series (<r²> vs time) for energy E = 4.0. The nonlinear relationship between t and r² indicates that the particle is not undergoing classical diffusion.

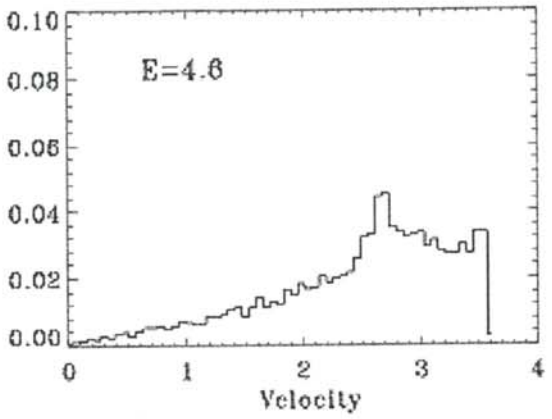

Figure 8
Velocity distribution function for energy E = 4.6. The structure of the VDF here, unlike that in Figure 4, is not consistent with each of the velocity components being a normally distributed random variable, suggesting non-Gaussian or anomalous diffusion.

$$\rho(t) = \langle (v_t)(v_{t+k}) \rangle . \tag{11}$$

The time it takes for the autocorrelation function value to approach zero represents the particle's "memory span." Since we are dealing with a numerical solution, we must use the discrete form of the autocorrelation function [7]:

$$\rho(t) = \sum_{t=1}^{N-1} (v_t)(v_{t+k}) . \tag{12}$$

We use the autocorrelation function to determine the power spectrum. A spectral analysis often provides a more general formulation of the system. To determine the power spectrum, S(ω), a Fourier transform was performed on the autocorrelation function [6]:

$$S(\omega) = \frac{1}{\pi} \int \rho(t) \cos(\omega t)\, dt. \tag{13}$$

We must keep in mind that our autocorrelation function is discrete, so again, the discrete form of the power spectrum

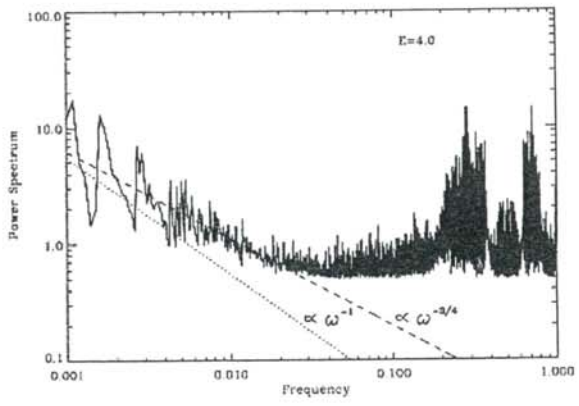

Figure 9
Power spectrum S(ω) for energy E = 4. The line $\omega^{-3/4}$ indicates the presence of the 1/f relationship as ω goes to 0.

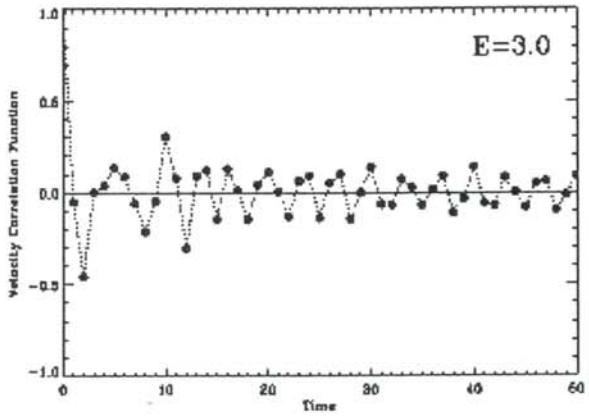

(a)

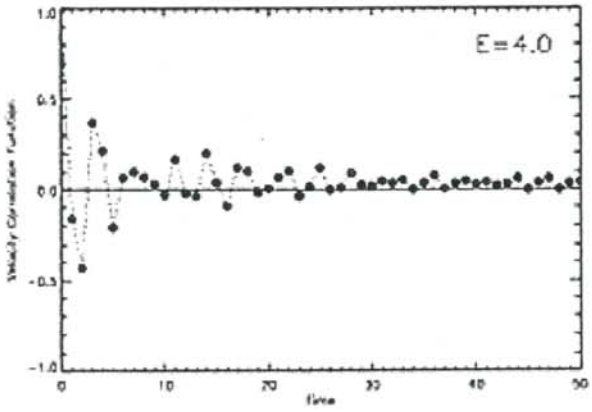

(b)

Figure 10
Velocity autocorrelation functions for energies (a) E = 3.0 and (b) E = 4.0.

is needed [7]. Rather than express it mathematically, we prefer to program it directly, as several complex numerical concepts such as windowing are needed to express it properly.

Figure 9 shows the power spectrum for $E = 4$. This analysis was performed on several energies between $E = 2$ and $E = 4.6$. We superimpose a line $S(\omega) = \omega^{-3/4}$ onto the spectrum shown in Figure 9, demonstrating a relative fit. This process was performed on the other energy levels in Table 1 as well. For the most part, each value corroborates the previous findings: the presence of $1/f$ noise[3].

E	α ($\pm$ 0.1)
2.5	0.8
3.0	0.7
4.0	0.75
4.25	1.0
4.35	1.1
4.6	1.0

Table 1
The exponent, α, values in the 1/f relationship for the power spectra at various energy levels [2].

$1/f$ noise, often called "flicker noise," is a characteristic that is closely related to the "memory span" of the particle as seen in the autocorrelation function [8]. By definition, observation of $1/f$ noise is related to the power spectrum by:

$$\lim_{\omega \to 0} S(\omega) = \frac{1}{\omega^{\alpha}}. \qquad (14)$$

Thus, $1/f$ noise emerges as t approaches infinity and is an intrinsic, property of the system. In the previous work, it is argued that *all* nonintegrable Hamiltonian systems display $1/f$ noise in their power spectra [3]. We have shown that this hypothesis is correct for the egg-crate potential.

Let us now return to the autocorrelation functions and explore further. Figure 10 shows the velocity autocorrelation functions for $E = 3.0$ and $E = 4.0$. As before stated, the autocorrelation function serves as a sort of graphical measure of the 'memory span' of the system and so. For a particle with a 'bad memory,' the autocorrelation function should go to zero fairly quickly. However, it should be noted that for our anomalously diffusing levels, the autocorrelation functions do not approach zero and remain there. Rather, the autocorrelation function seems to 'hover,' indicating that the particle retains a fair amount of knowledge about its initial velocity (which is related to both the initial energy and the initial position).

A log-log plot of the autocorrelation functions (Figure 11) reveals the presence of algebraic tails, sometimes referred to as long-time tails. Algebraic tails correspond to an algebraic decay in the correlation function as opposed to the exponential decay that is generally observed [9]. Thus, the presence of algebraic tails establishes definitively that

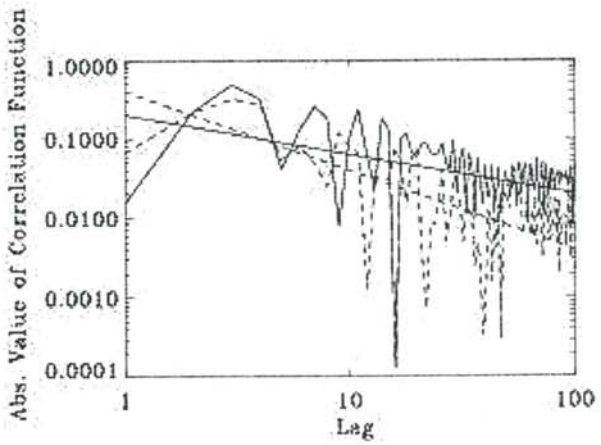

Figure 11
Velocity autocorrelation functions on a log-log scale to highlight the algebraic tail structure.

particles with energies between $E = 2$ and $E = 4.6$ have a long 'memory span' and possess more information about their previous velocities than is to be expected.

We now compare the autocorrelation functions with algebraic tails to each other in an attempt to further understand the nature of the time lags themselves. Initially, it was expected that tails relating to different anomalously diffusing energies were very similar. However, Fig. 12 depicts a histogram plot of the ratio of the autocorrelation functions at $E = 3$ and $E = 4.6$, again using our binning technique. For the most part, these functions are very comparable. But around step 16, there is a drastic difference between the functions, indicating that the algebraic tail observed at $E = 3$ is different in nature from the tail at $E = 4.6$. This is a surprising result that hints at an even higher complexity present in this system.

DISCUSSION

We have presented a thorough model and analysis of the motion of a classical particle in an egg-crate potential. It corroborates the research performed previously by T. Geisel and his group [3], thus providing an important validation of their work. This validation was necessary due to show that the numerical errors did not dominate the results. We feel confident in our results due to our care not to exceed the acceptable limits of error dictated by the standard deviation in Equation 6.

The presence of algebraic tails in the correlation functions of anomalously diffusing energies is a hallmark of chaos and is to be expected. However, the fact that different types of tails have been observed is not. It is currently unclear as to whether we are looking at different tails at every different energy or whether there exist subranges of energies that correspond to a certain family of tail. Further analysis will determine this.

The discovery of the presence of $1/f$ noise in the power spectra and distinct algebraic tails in the autocorrelation functions as a consequence of the motion of a classical particle in the egg-crate potential. It is important in future studies of chaotic Hamiltonian dynamics, establishing a prototype for the nonlinear Hamiltonian system and its statistical properties.

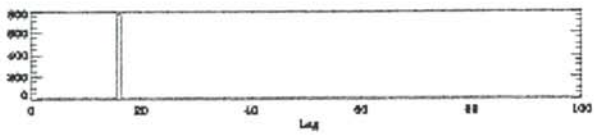

Figure 12
Histogram plot of the ratio between the velocity autocorrelation functions for energies E = 3.0 and E=4.6. The spike in the graph indicates that the algebraic tail at E = 3.0 differs signficiantly from the tail at E = 4.6, despite the fact that both energies exhibit anamalous diffusion.

ACKNOWLEDGMENTS

The author wishes to thank Dr. A.F. Barghouty for his encouragement and continuous support and the Roanoke College Summer Scholars Program for its generous financial support

REFERENCES

† current address of author: Physics Department, Cornell University, Ithaca, NY.
1. J. Klafter et. al., Physics Today, 49, (1996), pp. 33-39.
2. T. Geisel et. al., Phys. Rev. Lett., 59, (1987), pp. 2503-2506.
3. T. Geisel, Lévy Flights and Related Topics In Physics, M.F. Shlesinger, G.M. Zaslavsky, and U. Frisch, eds. Springer, Berlin, (1995), pp. 153-193.
4. J. Klafter et. al., *ibid*, pp. 196-215.
5. M. Tabor, Chaos And Integrability In Nonlinear Dynamics, John Wiley and Sons, New York, (1989), pp. 118-186.
6. M.J. Landahl and E. Mollo-Christensen, Turbulence and Random Processes in Fluid Mechanics: 2nd Edition, Cambridge UP, Cambridge, (1992), Chapter 4.
7. W.H. Press et al., Numerical Recipes in C: The Art of Scientific Computing, Cambridge UP, Cambridge, (1992), pp. 496-606.
8. Y.E. Kuzovlev, "Kinetical Theory Beyond Conventional Approximations and 1/f-noise," 1999, (Unpublished).
9. J. Stepisnik and P.T. Callaghan, Physica B, 292, (2000), pp. 296-301.

FACULTY SPONSOR

Dr. A.F. Barghouty
Dept. of Physics
Roanoke College
Salem, VA 24153
email: barghouty@urd.roanoke.edu

QUANTUM TUNNELING WITH MICROWAVES

Joel Moore
Department of Physics and Astronomy
University of Southern Mississippi
Hattiesburg, MS 39406-5046
Received July 24, 2002

ABSTRACT

Quantum tunneling is demonstrated in the form of 'frustrated total internal reflections' when $\lambda = 2.857$ cm microwaves tunnel through an air gap between two right angle prisms. For both orientations: transverse electric (TE) and transverse magnetic (TM); the transmissivity as a function of gap size agrees well with the theoretical predictions derived from electromagnetic theory.

INTRODUCTION

The concept of quantum tunneling is readily illustrated in superconductor physics by the 'Josephson effect', in which electrons from a superconducting metal tunnel through a thin layer of insulating material and produce current in the ordinary metal on the other side.[1] The tunneling decreases when the thickness of the insulating layer is increased. A similar manifestation of the quantum tunneling phenomenon occurs as electromagnetic radiation tunnels through a small gap in the material through which it is propagating. When visible light is incident on a crystal prism, the prism can be oriented such that the total internal reflection of light occurs, none of it escapes through the opposite side of the prism. Experiments [2,3], however, show that when a second prism is moved in close proximity to the first, such that the gap between them is on the order of the wavelength of the incident light, photons are able to tunnel through the air gap and propagate into the second prism, thus 'frustrating' the effect of total internal reflection.

The fraction of the total incident radiation that gets transmitted directly through the opposite side into the second prism, called the transmissivity, T, is given by:[4]

$$T = \frac{1}{1+A\sinh^2 bz}, \tag{1}$$

where:

$$b = \frac{2\pi}{\lambda}\sqrt{\frac{1}{2}n^2 - 1}\,, \tag{2}$$

is a constant depending on the refractive index of the prism, n, the wavelength of the incident radiation, λ, and z is the gap size. The constant A in Equation 1, in addition to being a function of n, is also dependent on the orientation of the electromagnetic fields of the incident waves with respect to the prism edges. When the electric field is oriented such that it oscillates at a constant angle with respect to the slanted surface of the prism (as shown in the Figure 1a), it is considered to be the Transverse Electric (or *TE*) orientation. If the orientation of the incident electric field is rotated 90°, such that the magnetic field oscillated parallel to the slanted surface, it is called the Transverse Magnetic (or *TM*) orientation (see Figure 1b).

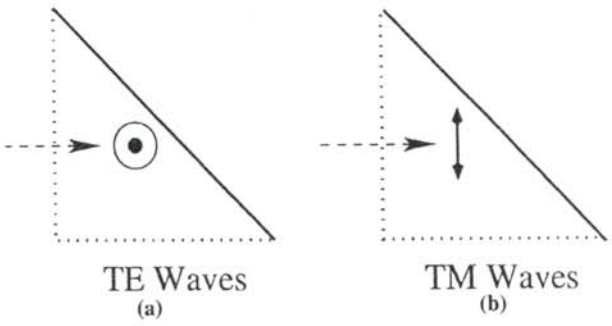

Figure 1
Schematic diagram showing the two polarizations: (a) the TE mode (electric field oscillates in and out of page); (b) the TM mode (electric field oscillates as shown).

Joel is a physics major at the University of Southern Mississippi. This research was done during his junior year as part of the required undergraduate curriculum. He currently is planning to attend graduate school to study thermodynamics. In his spare time, he enjoys cyclingt, kayaking, card games and swapping jokes with classmates and co-workers.

The expressions for A for these two orientations are given by: [4]

$$A_{TE} = \frac{\left(n^2-1\right)^2}{4\,n^2\cos^2\theta_i\left(n^2\sin^2\theta_i-1\right)}$$
$$A_{TM} = A_{TE}\left[\left(n^2+1\right)\sin^2\theta_i - 1\right], \qquad (3)$$

where θ_i is the angle of incidence of the electromagnetic beam on the prism. If θ_i is conveniently chosen to be 45°, Equations 3 become:

$$A_{TE} = \frac{\left(n^2-1\right)^2}{n^2\left(n^2-2\right)}$$
$$A_{TM} = \frac{\left(n^2-1\right)^4}{4\,n^2\left(n^2-2\right)} \qquad (4)$$

THE EXPERIMENT

For our experiment, we used the commercially available Pasco Gunn diode microwave transmitter and receiver. The output wavelength of the transmitter is 2.857 cm. The advantage of using this macroscopic wavelength is that the size of the gap between the two prisms (where the tunneling occurs) is easily measured and controlled. In the previously mentioned experiments using visible light, special equipment was required to measure the gap size, which could be as small as one wavelength: 500 to 700 nanometers.

We obtained two (45,45,90) paraffin prisms 30 cm along the sides by making wooden molds of he appropriate shape and filling them with molten parafin wax. Using a carpenter's plane, we honed the hypotenuse side of each prism so that the two fit together almost perfectly to form a cube. This assembly was then used to determine the index of refracdtion using aluminum foil to mask all but a 2 cm wide angular aperture on the microwave transmitter. The beam was aligned at an incident angle of 30° as shown in Figure 2. We detected a three-lobed diffraction pattern due to the aperture mask on the opposite side of the paraffin block. We took the middle of the center lobe to be the exit point and located that point. The index of refraction is obtained through Snell's law:

$$n = \frac{\sqrt{1+\left(\frac{L}{d}\right)^2}}{2}, \qquad (5)$$

where d is the distance between the entrance point and exit point of the beam and L is the length of one side of the cube. The results are shown in Table1. The index, n, is independent of the polarization of the microwaves.

We arranged the transmitter and the receivers at 90° angles with respect to the prisms as shown in Figure 3. One receiver was positioned to intercept the reflected portion of the signal, I_r, while the other received the transmitted portion, I_t. The distance from each receiver to the first diagonal face was the same. From the receiver readings, we obtained the transmissivity, T:

$$T = \frac{I_t}{I_t + I_r}. \qquad (6)$$

We began our data taking with the transmitter and receivers set to the *TE* polarization mode and set the gap size z = 2.4 cm. Values of I_r and I_t were recorded. z was then decreased in 2 mm increments until the two prisms touched. We repeated this procedure 5 times for each polarization.

RESULTS AND DISCUSSION

Our results are shown in Figure 4 for both polarization modes. The solid lines are the theoretical results using Equation 1 and the values from Table 1. The theoretical curves matched the data for the *TE* waves quite well. For the *TM* waves, however, the theoretical values were larger than the experimental values.

We noticed that the value of I_t never became zero, even when z was extended to lengths where total internal reflections should occur. There are a couple of possible explanations for why this occurred.

One possible explanation for the non-zero value of I_t, lies in the quality of the prism material. The prism was made by melting paraffin and pouring it into a mold, thereby aerating the molten liquid , producing tiny air bubbles in

	$n = 1.56\pm0.02$	
$b = 1.02\pm0.01$	$A_{TE} = 1.95\pm0.05$	$A_{TM} = 1.0\pm0.1$

Table 1
Values for the constants (from Equations 2 and 4) used in the curve fits of Figure 4.

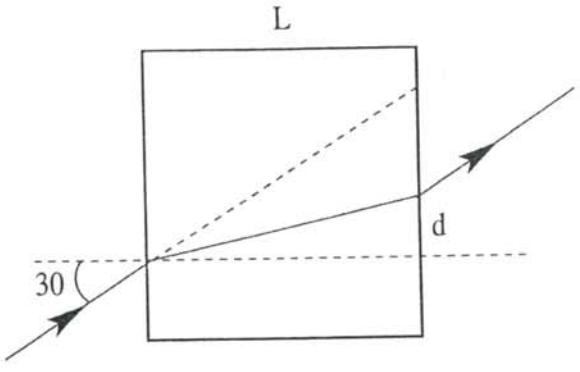

Figure 2
Schematic diagram of paraffin blocks showing how we measured the index of refraction

the finished product. These bubbles, although not large enough to alter the path taken by the microwave, may have produced tiny areas that offered very little impedance to the incoming electromagnetic wave, resulting in a slightly higher transmissivity than predicted. These bubbles might be particularly troublesome when they happen to be located on the reflecting surface of the prism. The plausibility of this explanation is reinforced by one of our earlier experiments where we used a prism consisting of a thin foam-board container of the appropriate shape filled with polystyrene pellets. This method resulted in innumerable air gaps between the pellets. The transmissivity was so high that is made small changes in the reflection and transmission difficult to observed. An identical experiment using polyethylene pellets yielded similar results and forces us to abandon this type of prism in favor of one made of solid paraffin.

A possible explanation for the persistent nonzero reading for I_t is that the transmitters and receivers were equipped with horns that spread the signal at approximately 30° for the *TE* mode and 60° for the *TM* orientation. This made it possible for part of the signal to enter the incident face of the prism at an angle of other than 90° and strike the slanted face of the prism at an angle less than the critical angle for total internal reflections, thus transmitting the signal to the second prism.

ACKNOWLEDGMENTS

The author would like to thank Professor William Hughes for his assistance with the microwave equipment and Mr. Richard Canty of the University of Southern Mississippi carpentry shop for his assistance in making the prisms. Lastly, help from Hancock High School student Randall Dannemann was greatly appreciated.

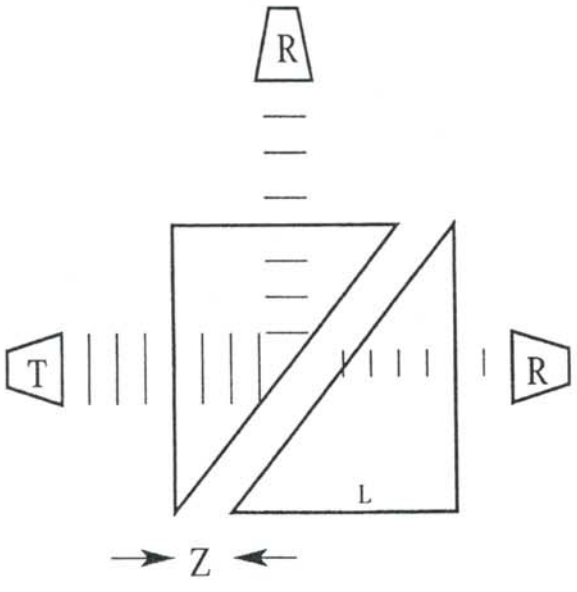

Figure 3
Experimental Configuration. T is the microwave transmitter. The upper receiver R records the reflected intensity, the right receiver records the transmitted intensity.

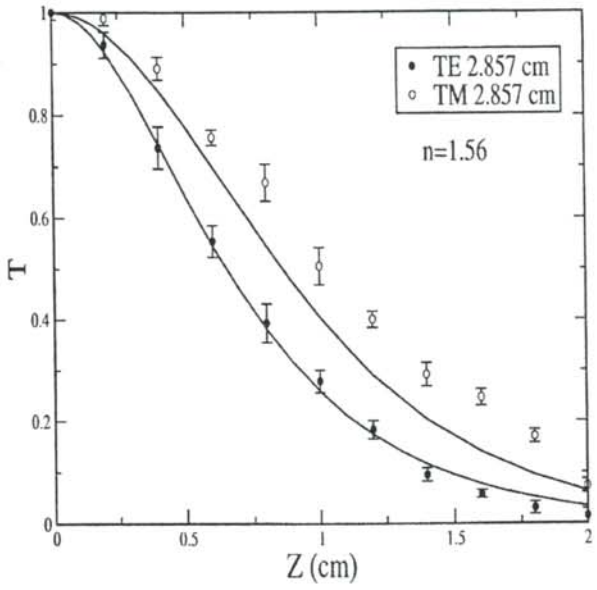

Figure 4
Transmissivity versus Gap Size. The solid lines are the corresponding theoretical curves given in Equations 3.

REFERENCES

1. C. Kittel, Introduction to Solid State Physics, 4th Ed., John Wiley & Sons, (1971), ppl. 435 - 437.
2. A. Kodre and J. Strnad, Am. J. Phys., 44, (1976), pp. 181-182.
3. M.K. Handy and G.F. Landegrin, Am. J. Phys., 45, (1977).
4. R.H. Good and T.J. Nelson, Classical Theory of Electric and Magnetic Fields, Academic Press, N.Y., (1971), pp. 380-383.

FACULTY SPONSOR

Dr. Lawrence R. Mead
Department of Physics
University of Southern Mississippi
Hattiesburg, MS 39406-5046
Lawrence.Mead@usm.edu

AN EXPERIMENTAL STUDY OF STICK-SLIP FRICTION USING SANDPAPER AS A SIMPLE MODEL OF EARTHQUAKE DYNAMICS

Jason Foust†
Department of Chemistry and Physics
Mansfield University
Mansfield, PA 16933
received June 1, 2002

ABSTRACT

An experimental study of stick-slip friction was conducted using sandpaper and paper towels. This study models stick-slip friction earthquakes. A block with sandpaper on its bottom was fixed to a strain gauge by means of a spring. A paper towel was pulled beneath the block, stretching the spring, while the position of the block was monitored with a linear displacement gauge. Readings from the strain gauge and linear displacement gauge then were used to determine the energy released when the block slid backwards. Analysis of the data suggests that the interaction of the sandpaper with the paper towel depends on both the sandpaper grit size and the surface roughness of the paper towel.

INTRODUCTION

Earthquakes can cause severe social and economic impact on communities. While it is unknown if earthquake prediction will ever be possible, a better understanding of what earthquakes has been developed. Production of stresses in adjacent plate regions is the ultimate cause of earthquakes. The varying stresses cause the Earth's surface to move differently. The most common cause of earthquakes is the breaking of rocks beneath the surface of the Earth due to various geological forces. [1] Volcanic theory proposes an explanation based on explosive chemicals or the sudden stoppage of magma flow [2] Earthquakes also can be caused by cavern and mine decay, massive landslides and the detonation of nuclear weapons can trigger an earthquake. [3]

One type of earthquake is caused by the motion of tectonic plates along fault lines, such as occurs along the notorious San Andreas Fault. For earthquakes of this type, which occur in other parts of California and Japan, the Earth's tectonic plates move both horizontally and vertically in measurable amounts. [2] This motion gives rise to the phenomenon known as stick-slip friction. Stick-slip friction is the cyclic transition from static friction to kinetic friction at slow speeds. The condition lasts until enough shear stress is built up to overcome the static friction, allowing the surfaces to break apart. During this process of separation, one surface slides back and releases energy. [4]

A previous study of stick-slip friction suggests that the greater the surface roughness, the longer the time elapsing between the slip events and the greater the energy buildup and subsequent energy release. [5] Based on this, it is expected that the degree of surface roughness and the energy release during the earthquake are related since the building up of the shear force continues until the static frictional force is overcome and the sliding begins.

THE EXPERIMENT

The apparatus used to model the stick-slip friction is shown in Figure 1. A seamless paper towel was pulled across the track at an average speed of 0.5 mm/s by a constant angular speed motor. This speed was chosen so that so that small slip-events would not be missed. Resting on top of the towel was an aluminum block with sandpaper glued to the bottom. This block was attached to a strain gauge by means of a spring. A linear displacement

Jason has completed his undergraduate degree in physics at Mansfield University. He is currently pursuing his master's degree in mechanical engineering at Lehigh University. When Jason is not in the lab or in the library studying for a test, he likes to spend time playing basketball and lifting weights with his fellow classmates.

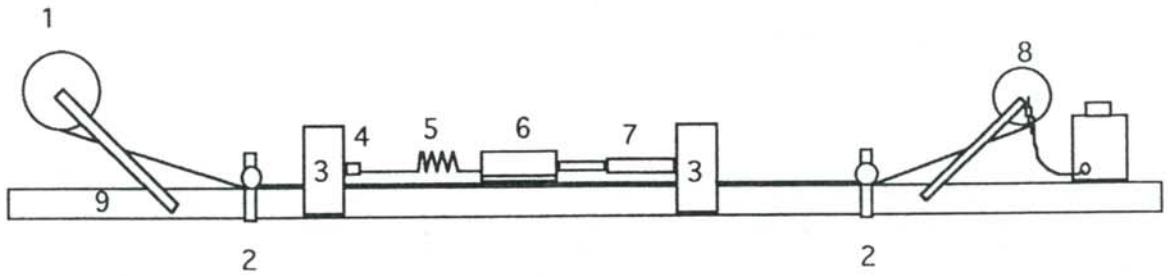

Figure 1
A schematic diagram of the stick-slip friction apparatus: (1) paper towel roll; (2) paper flattening rollers; (3) support frame; (4) strain gauge; (5) spring; (6) metal block with sand paper bottom; (7) linear displacement gauge; (8) paper collector spool and motor; (9) polished track.

gauge was used to measure the position of the block. As the paper towel was pulled from left to right (see Figure 1), the block was pulled along until the spring restoring force was sufficient to overcome the static frictional force. When this occurred, the block slipped back.

The strain gauge was used to determine the equilibrium position of the block and to establish the linearity of the spring restoring force with spring stretch. The linear displacement gauge was used to determine the position of the block. The output voltage from the linear displacement gauge was sent to an analog to digital data acquisition card in a computer. Data for a given run were acquired every 0.2 s for a total sampling time of 500 s. This sampling time was chosen for several reasons. As more paper towel accumulated on the collector spool, its radius increased. The motor shaft driving the collector spool rotated with constant angular speed, so this increase in radius resulted in an increasing translational speed of the paper towel passing beneath the block as the paper towel moved. The sampling time was kept short to minimize the variation in the speed of the paper towel. A longer sampling time would also affect the sandpaper and paper towel. Preliminary runs revealed a build-up of paper towel on the sandpaper for longer sampling times. A sampling time of 500 s did not eliminate this build-up, but it did minimize it.

The surface roughness was varied by using sandpaper of a variety of grit numbers, ranging from 150 to 2000. Sandpaper grit number is a measure of the size of the abrasive particles attached to the sandpaper backing. Low grit number sandpaper has larger abrasive particles, so it is coarser than high grit number sandpaper. Table 1 shows the different sandpaper grit numbers used in this study and the corresponding abrasive particle sizes. 6

The sandpaper beneath the aluminum block was replaced with a new piece after two runs. Block positions versus time for twenty runs (10 new pieces of sandpaper) were acquired for each of the grits listed in Table 1. Data from the odd numbered runs (the ones with the fresh sandpaper) were compared with data from the even numbered runs (second time around for the sandpaper) to determine if the paper towel buildup was affecting the results. No significant difference between runs was observed, indicating that

Grit Number	Abrasive Particles Average Grit Diameter (μm)
150	93.0
180	78.0
240	53.5
360	28.8
400	23.6
600	16.0
P1000	12.6
P1500	10.3
1000	9.2

Table 1
Average size of abrasive particles for the various sandpaper grit numbers [6] used in this study.

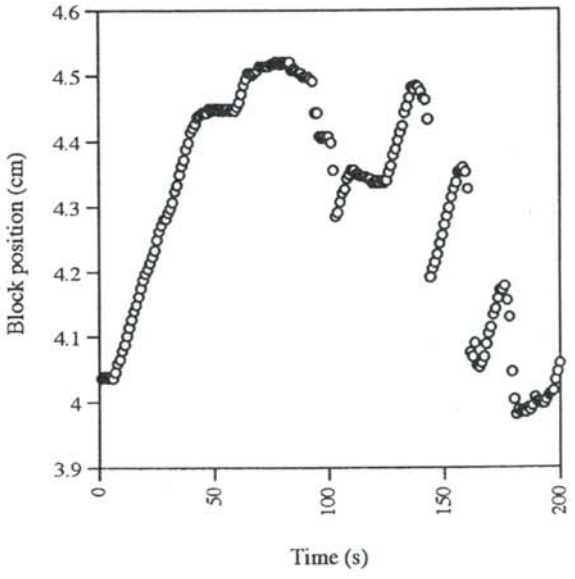

Figure 2
Block position as a function of time for the first 40 s of a run using 240 grit sandpaper.

the sandpaper and paper towel interactions for all runs of a given sandpaper grit number were similar.

DATA AND ANALYSIS

The position versus time data from each run were analyzed to determine when the slip events took place. A plot of block position versus time for the first 40 s of a run for the 240 grit sandpaper is shown in Figure 2. The peaks represent the maximum spring stretch prior to slipping. The valleys are when the block has slid back maximally. The difference in energy between the peak spring stretch and the valley spring stretch is the energy released when the block slid back. A sorting program was written and used to determine when slip events occurred and to calculate the energy released during such events. The slip energies for each run for a given sandpaper grit number were combined into a single data set. Another program then was used to sort the data into bins so that a histogram of the number of slip events as a function of slip energy could be made. Figure 3 shows the number of slip events as a function of the energy for the 240 and 360 grit sandpaper. The decrease in the number of slip events with increasing slip energy was observed for all sandpaper grit sizes tested.

The shape of the histogram plots shown in Figure 3 suggests an decreasing exponential dependence of the number of slip events in the increasing slip energy. In keeping with the tradition that base 10 logarithms are used in earthquake studies, the data were fit with an exponential of the form:

$$N = N_0\, 10^{-\alpha E}, \qquad (1)$$

where N is the number of slips, No and α are curve fit parameters, and E is the slip energy. If the functional form of Equation 1 adequately describes the histogram plots in Figure 3, a plot of $\log_{10}(N)$ versus E should yield a line with a slope equal to $-\alpha$. The semi-log plots for the 360 and 1000 grit sandpaper, shown in Figure 4, support this dependence. The straight lines shown in Figure 4 are linear fits to the data points.

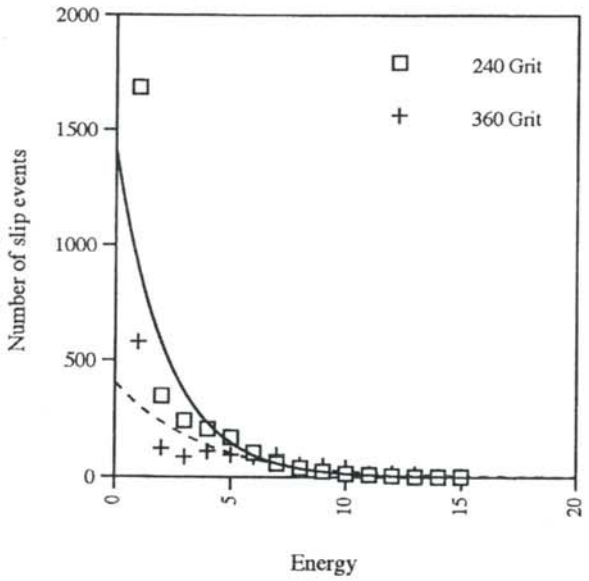

Figure 3
Number of slip events versus the energy released per slip for 240 (open square) and 360 (cross) grit sandpaper.

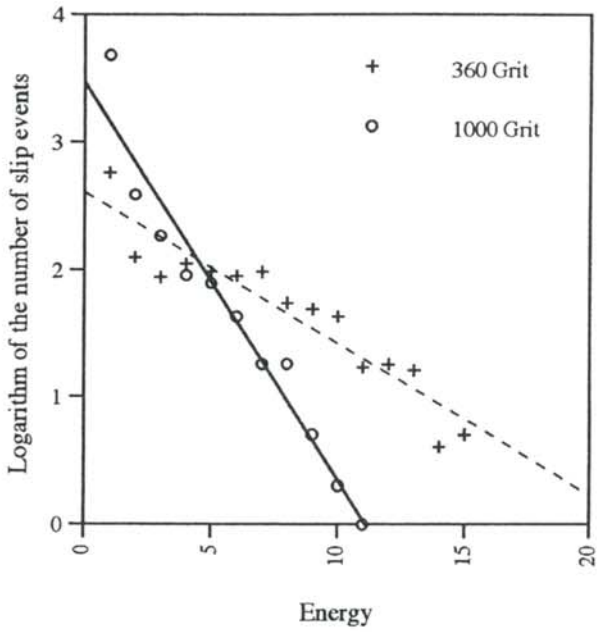

Figure 4
Logarithm of the number of slip events versus the energy released per slip for 360 (cross) and 100 (open circle) grit sandpaper. The lines shown are linear fits to the data points.

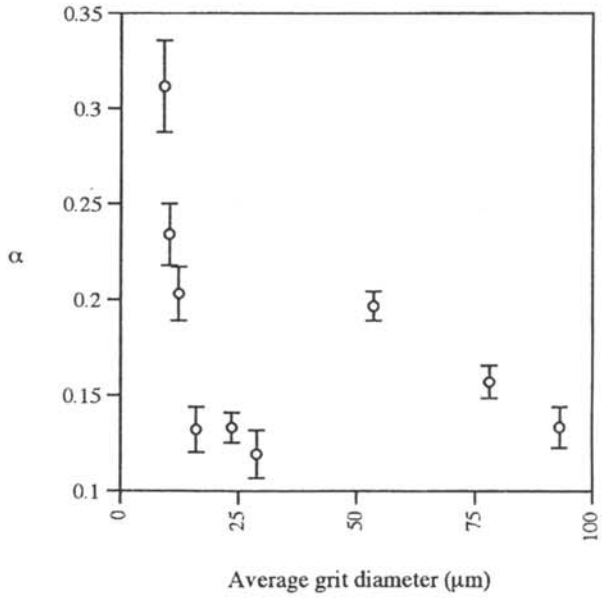

Figure 5
Plot of the α values versus the average grit diameter

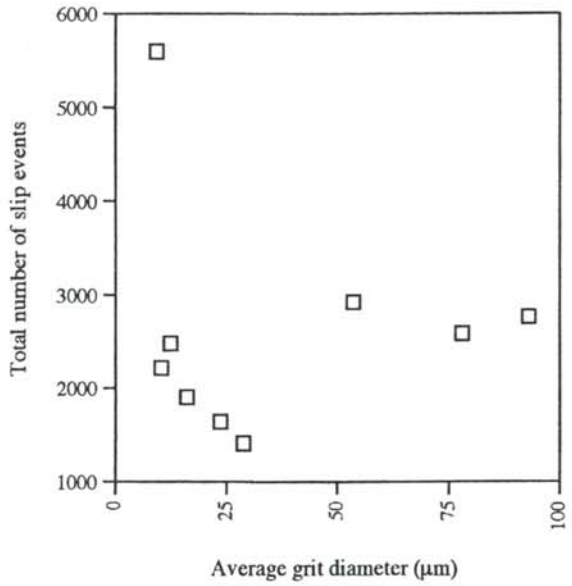

Figure 6
Total number of slip events versus the average grit diameter.

We expected that the rougher sand paper (that with lower grit number and larger average abrasive particle size) would have more large energy slip events than the smoother sandpaper. If this were true, then α would be smaller for the large grit sandpaper than for the small grit sandpaper. A plot of the α values as a function of average grit diameter is shown in Figure 5. The sandpaper with the largest particles did have a smaller value of a than the sandpaper that had the smallest particles, but the middle grit sized sandpaper generally had the smallest α values.

More insight into what may be happening can be gleaned by examining Figures 6 and 7. In Figure 6, the number of slip events as a function of abrasive particle size is plotted. The number of slip events follows a trend similar to those observed in the a values. The average energy released for each slip event is plotted as a function of abrasive grit size in Figure 7. Sandpaper with midsize grit particles results in larger average slip energies than sandpaper with finer and coarser grit

One possible explanation of the behavior seen in our results is that the interactions of the sandpaper with the paper towel depends not only on sandpaper grit size, but also on the surface roughness of the paper towel. The paper towel used was not perfectly smooth; it contained randomly spaced paper fibers as well a regularly spaced, but randomly high protrusions. Three possible interaction systems are illustrated in Figure 8. The course sand paper had particles that may have been too large to effectively interact with the crevices in the paper towel. The fine sandpaper had abrasive particles that may have been too small to fit in the paper towel crevices. Finally, the mid-ranged sandpaper abrasive particles may have been just the right size to fall into the voids between the paper fibers.

It is unclear if the results of this study can help to shed

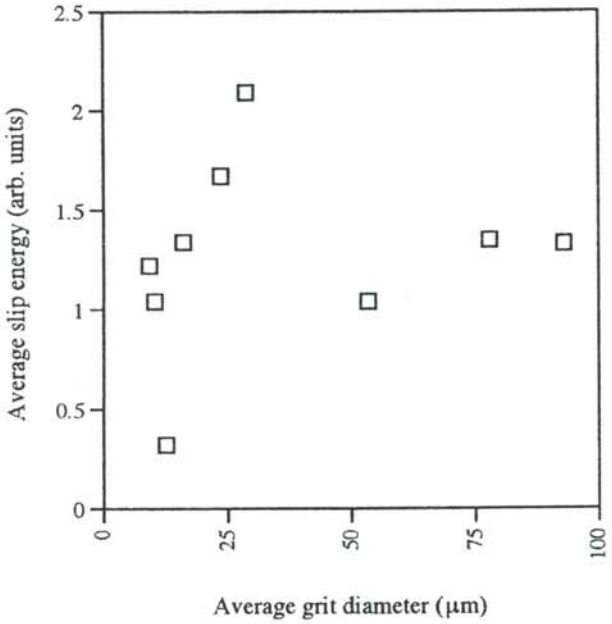

Figure 7
Plot of the average slip energy versus the average grit diameter.

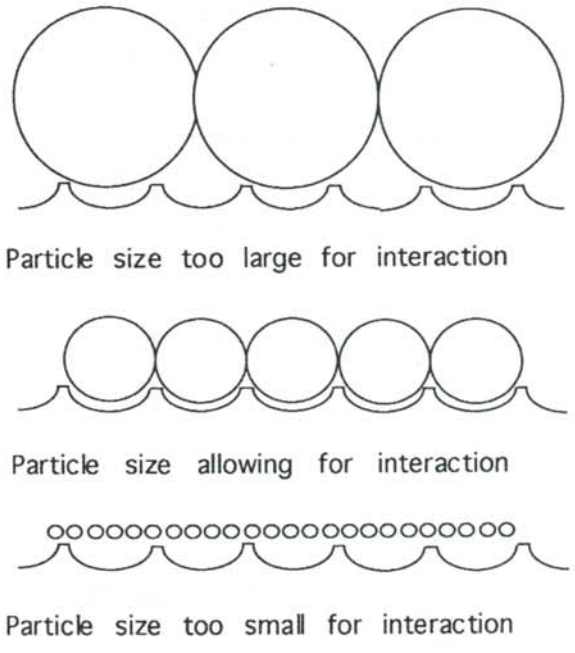

Figure 8
Diagram showing the three possible scenario for interactions between the sand paper abrasive particles and the paper towel.

light on what happens during real stick-slip earthquakes. It is interesting, however, that the distribution of slip events in this study obeys the same exponential law that is observed for real earthquakes. [7]

ACKNOWLEDGMENTS

The author would like to thank Dr. Michael Chester for his guidance and advice throughout this project. He thanks the Department of Chemistry and Physics for providing the necessary resources.

REFERENCES

† current address of author: Department of Mechanical engineering and Mechanics, Packard Laboratory, Lehigh University, Bethlehem, PA 18015.

1. B.A. Bolt, Earthquakes, W.H. Freeman, New York, (1933), p. 98.
2. N.H. Heck, Earthquakes, Hafner, New York, (1965), pp. 30-34.
3. B.A. Bolt, Earthquakes and Volcanoes, W.H. Freeman, New York, (1980), p. 2.
4. R.J. Twiss and E.M. Moores, Structural Geology, W.H. Freeman, New York, (1973), p. 176.
5. J.H. Dietrich, Pure Appl. Geophys., 116, (1978), pp. 790-806.
6. There are two different standards in use for denoting abrasive particle size. Sandpaper without a letter in front of the grit number follows the U.S. standard, while sand paper with a *P* in front of the grit numbers follows the European standard.
7. B. Gutenberg and C.F. Richter, Ann. Geofis., 9, (1956), p.1.

FACULTY SPONSOR

Dr. Michael J. Chester
Department of Chemistry and Physics
Mansfield University
Mansfield, PA 16933

A MODEL FOR THE MOTION OF A KINETIC MOBILE

Brian Bockelman †
Department of Physics
State University of West Georgia
Carrollton, GA 30118
received April 15, 2002

ABSTRACT

The 'cosmic ring kinetic mobile' is a device that involves a systems of weights and rings, hung at angles to produce visually stimulations motions, that is driven by a electromagnet. We simplify the system by considering the behavior of one of the rings and arrived at a system of equations that describe the motion. Properly chosen coordinate transformations make it possible to understand the motion in a mathematically simple manner. We derive the equations of motion, a set of nonlinear coupled second order differential equations, and present numerical results obtained by considering various limits of the motion, as well as the full set of equations. The limiting forms of the equations are harmonic.

THE MODEL

The kinetic mobile, shown in Figure 1, is a deceptively simple looking device, arranged with increasingly smaller rings attached to a string by a thin wire, each hanging at a certain angle. In the middle of all of the rings is a spherical weight. At the bottom of the sing is a conical electromagnet that drives the motion, compensating for the drag force. These rings spin complicated patterns. To model their entire motion is very complex.

Instead, we model the motion of a single ring as shown in Figure 2. The curved piece of wire connecting the ring to the string is assumed to be massless, so we need only consider the affects of the string on the ring. No external forces, such as the driving or drag forces are considered.

The Inertia Tensor

To obtain the equations of motion of the system, we first determine the moment of inertia tensor. As the ring does not lie on or spin about its principle axis, we have calculate all the elements of the tensor. We calculated the inertia tensor in 'body coordinates' and write the torques and angular acceleration in a rotating coordinate system

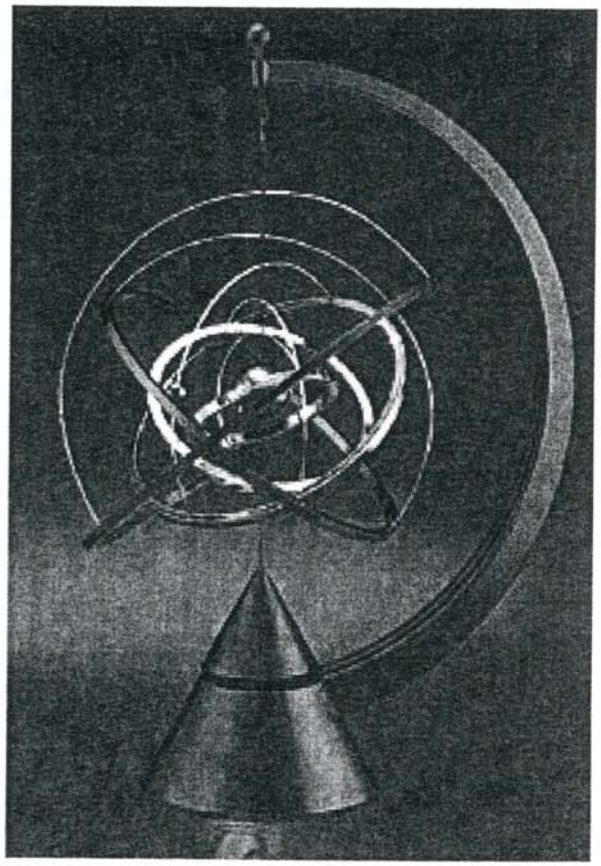

Figure 1
A picture of the actual 'cosmic ring kinetic mobile' (see reference 6)

Brian is a junior at the State University of West Georgia, and a senior at South Gwinnet High School. He plans to major in mathematics. This research project began during the fall semester of his freshman year. He is currently preparing this project for a poster session of the National Collegiate Honors Council and another project for the AMS meeting in January. In his spare time, he can be found tutoring students and hanging with his friends.

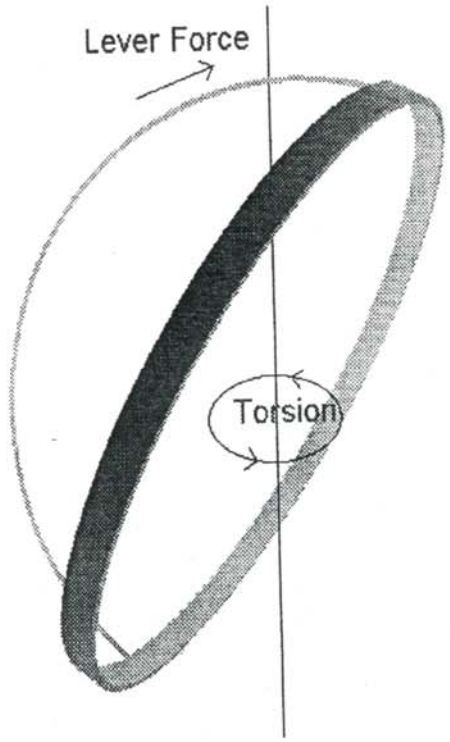

Figure 2
A one ring system used as a simplified model of the full system shown in Figure 1

which we call 'world coordinates', then finally rotate the torque and acceleration back to 'body coordinates' to obtain the equations of motion.

The moment of inertia of the ring in body coordinates (along the principal axis) is: [1]

$$I_b = \begin{bmatrix} \rho\int (y^2+z^2)\,dV & 0 & 0 \\ 0 & \rho\int (x^2+z^2)\,dV & 0 \\ 0 & 0 & \rho\int (x^2+y^2)\,dV \end{bmatrix} \quad (1)$$

The 'body coordinates' are those for which the ring is placed 'flat' on the x-y plane. The moment of inertia in world coordinates would have non-zero off-diagonal elements in the matrix. Fortunately, the body coordinates of the moment of inertia tensor is all that we will need. Both the body and the world coordinate systems are shown in Figure 3.

To transform between the two coordinate systems [1 one] uses the orthogonal rotation matrix given by:

$$\lambda = \begin{bmatrix} \cos\phi & 0 & \sin\phi \\ 0 & 1 & 0 \\ -\sin\phi & 0 & \cos\phi \end{bmatrix}, \quad (2)$$

Equation 2 is the form for a rotation about the y-axis by angle ϕ.[2]

The torque, τ, the inertia tensor, I, and the angular acceleration, α, can be written as:

$$\vec{\tau}_w = \lambda \cdot \vec{\tau}_b, \quad I_w = \lambda \cdot I_b \cdot \lambda^{\dagger}, \quad \vec{\alpha}_w = \lambda \cdot \vec{\alpha}_b \quad (3)$$

where the subscript w stands for the world coordinates and the subscript b stands for the body coordinates.

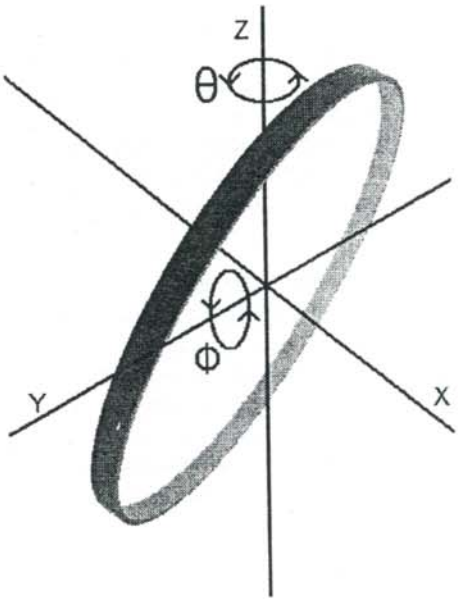

(a) world coordinates

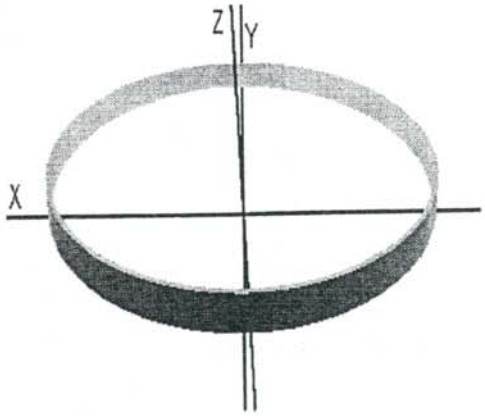

(b) body coordinates

Figure 3
An illustration of the difference between body and world coordinates. (a) world coordinates. (b) Body coordinates

Due to the symmetry of the ring, the diagonal components of I_b (Equation 1) can be calculated using cylindrical coordinates ($x = r\cos\theta$, $y = r\sin\theta$):

$$\begin{aligned}
(I_b)_{11} &= \int_0^h \int_0^{2\pi} \int_{r_1}^{r_2} (y^2 + z^2)\, r\, dr\, d\theta\, dz \\
&= \rho\left[\frac{\pi h^3 (r_2^2 - r_1^2)}{3} + \frac{\pi h (r_2^4 - r_1^4)}{4}\right] \\
(I_b)_{22} &= \int_0^h \int_0^{2\pi} \int_{r_1}^{r_2} (x^2 + z^2)\, r\, dr\, d\theta\, dz \\
&= \rho\left[\frac{\pi h^3 (r_2^2 - r_1^2)}{3} + \frac{\pi h (r_2^4 - r_1^4)}{4}\right] \\
(I_b)_{33} &= \int_0^h \int_0^{2\pi} \int_{r_1}^{r_2} (x^2 + y^2)\, r\, dr\, d\theta\, dz \\
&= \rho\left[\frac{\pi h (r_2^4 - r_1^4)}{2}\right],
\end{aligned} \tag{4}$$

where r_1 and r_2 and the inner and outer radii of the ring, h is the thickness of the ring, ρ is the density (assumed to be constant) and:

$$\rho = \frac{m}{V}, \quad V = \pi h (r_2^2 - r_1^2), \tag{5}$$

Equations 4 can be combined with Equation 5 to give the moment of inertia in the body coordinate system:

$$I_b = \begin{bmatrix} m\left(\frac{h^2}{3} + \frac{r_2^2 + r_1^2}{4}\right) & 0 & 0 \\ 0 & m\left(\frac{h^2}{3} + \frac{r_2^2 + r_1^2}{4}\right) & 0 \\ 0 & 0 & m\left(\frac{r_2^2 + r_1^2}{2}\right) \end{bmatrix}. \tag{6}$$

Equations of motion

The string exerts two torques on the ring: a torsional torque, ttors, in the z-direction and 'lever torque', tlever, to keep the ring in its upright position. The torsional torque is modeled in terms of Hooke's Law for spring motion.[3] In world coordinates:

$$\overrightarrow{\tau_{tors,w}} = \begin{bmatrix} 0 \\ 0 \\ -k_1\theta \end{bmatrix}. \tag{7}$$

To transform the torsional torque into body coordinates one must use the adjoint of the rotation matrix (Equation 2):

$$\overrightarrow{\tau_{tors,b}} = \lambda^\dagger \cdot \overrightarrow{\tau_{tors,w}} = \begin{bmatrix} k_1\theta\sin(\phi) \\ 0 \\ -k_1\theta\cos(\phi) \end{bmatrix}. \tag{8}$$

As the ring rotates, a torque is applied to change ϕ from its initial position ϕ_o, the string reacts in the opposite way. Once again, we model this torque in the form of Hooke's Law:

$$\overrightarrow{\tau_{lever,w}} = \begin{bmatrix} 0 \\ -k_2(\phi - \phi_o) \\ 0 \end{bmatrix}. \tag{9}$$

Transforming this torque to body coordinates:

$$\overrightarrow{\tau_{lever,b}} = \lambda^\dagger \cdot \overrightarrow{\tau_{lever,w}} = \begin{bmatrix} 0 \\ -k_2(\phi - \phi_o) \\ 0 \end{bmatrix}. \tag{10}$$

The net torque in the body coordinates acting on the ring is the sum of torques in Equations 8 and 10:

$$\overrightarrow{\tau_{net,b}} = \begin{bmatrix} k_1\theta\sin(\phi) \\ -k_2(\phi - \phi_o) \\ -k_1\theta\cos(\phi) \end{bmatrix}. \tag{11}$$

According to Newton, the net torque is the time rate of change of the angular momentum:

$$\overrightarrow{\tau_{net,b}} = \frac{d\vec{L}_b}{dt}, \tag{12}$$

where:

$$\vec{L}_b = I_b \cdot \vec{\omega}_b, \tag{13}$$

and:

$$\vec{\omega}_b = \lambda^\dagger \vec{\omega}_w. \tag{14}$$

The angular velocity in the world coordinate system is given by:

$\phi(0) = \pi/3$	$\phi'(0) = 2$
$\theta(0) = 5$	$\theta'(0) = 3$
$k_1 = .001$	$k_2 = .1$
$r_2 = .0500$	$r_1 = .0495$
$m = .05$	$h = .005$

Table 1
Numerical values for the various parameters used in the numerical solutions.

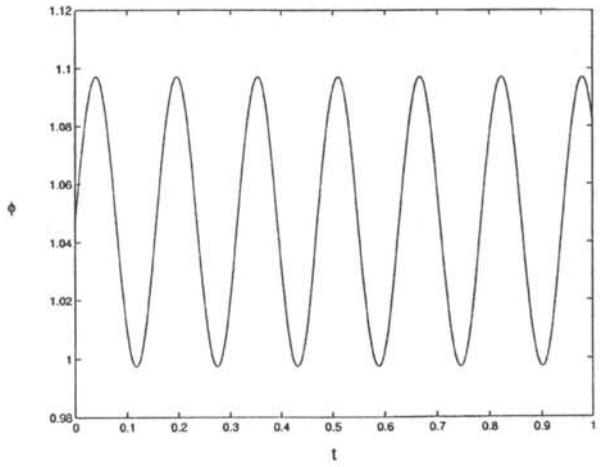

Figure 4
A graph of $\phi(t)$ as a function of time. Points are those produced by the numerical solution to Equation 22a.

$$\vec{\omega}_w = \begin{bmatrix} 0 \\ \frac{d\phi}{dt} \\ \frac{d\theta}{dt} \end{bmatrix} \tag{15}$$

where ϕ and θ are shown in Figure 3. Transforming the angular velocity to the body coordinate system:

$$\vec{\omega}_b = \begin{bmatrix} -(\sin\phi)\frac{d\theta}{dt} \\ \frac{d\phi}{dt} \\ (\cos\phi)\frac{d\theta}{dt} \end{bmatrix}. \tag{15}$$

Combining Equations 11-16, we find that:

$$\frac{dL_b}{dt} = \begin{bmatrix} -(I_b)_{11}\left\{\cos\phi\,\frac{d\phi}{dt}\,\frac{d\theta}{dt} + \sin\phi\,\frac{d^2\theta}{dt^2}\right\} \\ (I_b)_{22}\,\frac{d^2\phi}{dt^2} \\ -(I_b)_{33}\left\{\sin\phi\,\frac{d\phi}{dt}\,\frac{d\theta}{dt} - \cos\phi\,\frac{d^2\theta}{dt^2}\right\} \end{bmatrix} = \begin{bmatrix} k_1\theta\,(\sin\phi) \\ -k_2(\phi-\phi_o) \\ -k_1\theta\,(\cos\phi) \end{bmatrix}. \tag{16}$$

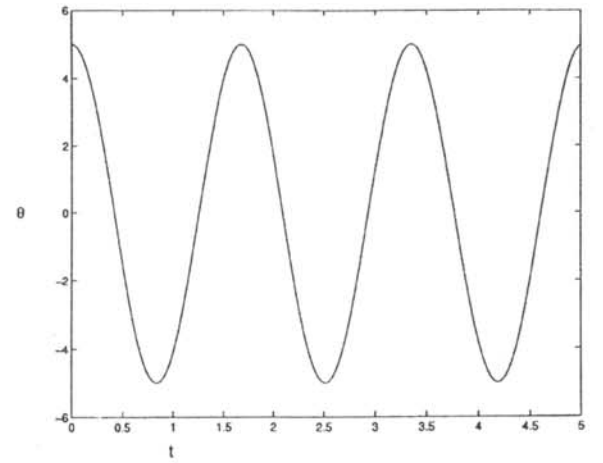

Figure 5
A graph of $\theta(t)$ versus time. The points are the numerical solution to Equation 22b using the values in Table 1.

where $(I_b)_{11}$, $(I_b)_{22}$, and $(I_b)_{33}$ are the diagonal elements of the moment of inertia tensor shown in Equation 6. From the three different expressions for the net torque in Equation 16 we can extract the equations of motion of the ring:

$$(\sin\phi)\,\frac{k_1}{(I_b)_{11}}\theta = -\cos\phi\,\frac{d\phi}{dt}\,\frac{d\theta}{dt} - \sin\phi\,\frac{d^2\theta}{dt^2} \tag{17}$$

$$\frac{k_2}{(I_b)_{22}}(\phi-\phi_o) = -\frac{d^2\phi}{dt^2} \tag{18}$$

$$(\cos\phi)\,\frac{k_1}{(I_b)_{33}}\theta = \sin\phi\,\frac{d\phi}{dt}\,\frac{d\theta}{dt} - \cos\phi\,\frac{d^2\theta}{dt^2} \tag{19}$$

The equations of motion are a coupled, second order nonlinear system of equations. However, there are three equations for only two variables. The non-linear term in Equations 17 and 19 can be eliminated by multiplying equation 17 by sinϕ and Equation 19 by cosϕ and subtracting:

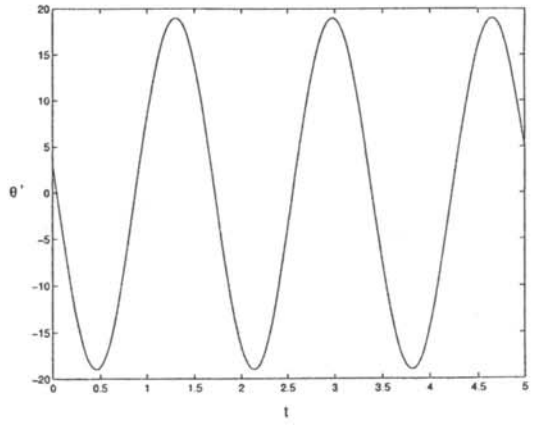

Figure 6
A graph of $\frac{d\theta}{dt}$ versus time.

$$\frac{d^2\theta}{dt^2} = -k_1\left\{\frac{\sin^2\phi}{(I_b)_{11}} + \frac{\cos^2\phi}{(I_b)_{33}}\right\}\theta. \qquad (20)$$

or:

$$\frac{d^2\theta}{dt^2} = -k_1\left\{\left(\frac{1}{(I_b)_{11}} - \frac{1}{(I_b)_{33}}\right)\sin^2\phi + \frac{1}{(I_b)_{33}}\right\}\theta \qquad (21)$$

So, the equations of motion of the system become:

$$\frac{d^2\phi}{dt^2} = -\frac{k_2}{(I_b)_{22}}(\phi - \phi_o) \qquad (22a)$$

$$\frac{d^2\theta}{dt^2} = -k_1\left\{\left(\frac{1}{(I_b)_{11}} - \frac{1}{(I_b)_{33}}\right)\sin^2\phi + \frac{1}{(I_b)_{33}}\right\}\theta \qquad (22b)$$

Note that Equation 22a is the simple harmonic oscillation equation.

Special cases of the motion

Equation 22a is the simple harmonic oscillator equation. The solution is of the form:

$$\phi(t) = \left[\frac{d\phi}{dt}(0)\right]\sqrt{\frac{(I_b)_{22}}{k_2}}\sin\left(\sqrt{\frac{k_2}{(I_b)_{22}}}\,t\right) + \frac{\pi}{3}. \qquad (23)$$

Equation 22b can be linearized by making assumptions about $\phi(t)$. If $\phi(t)$ varies so slowly or the amplitude term in front of the sine function in Equation 23 is very small, it can be considered a constant. Then, using the values of the parameters shown in Table 1, equation 22b can be written as:

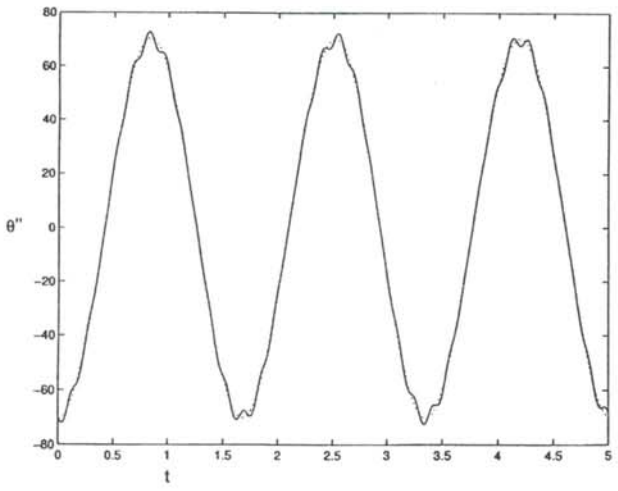

Figure 7
A graph of the full numerical solution of $\theta''(t)$ versus time (solid) and the limiting case version of the second time derivative of Equation 25 (dashed).

$$\frac{d^2\theta}{dt^2} = -k_1\left\{\left(\frac{1}{(I_b)_{11}} - \frac{1}{(I_b)_{33}}\right)\sin^2\left(\frac{\pi}{3}\right) + \frac{1}{(I_b)_{33}}\right\}\theta$$

$$= -\frac{k_1}{4}\left(\frac{3}{(I_b)_{11}} + \frac{1}{(I_b)_{33}}\right)\theta, \qquad (24)$$

a harmonic oscillator with the solution:

$$\theta(t) = \frac{\frac{d\theta}{dt}(0)}{k_3}\sin(k_3 t) + \theta(0)\cos(k_3 t), \qquad (25)$$

where

$$k_3 = \sqrt{\frac{k_1}{4}\left(\frac{3}{(I_b)_{11}} + \frac{1}{(I_b)_{33}}\right)}. \qquad (26)$$

However, to understand the proper motion of this system, we investigate them using numerical techniques.

RESULTS

We generated numerical solutions of Equations 22 using Mathematica [4] and Matlab6 [5]. A listing of the programs capable of generating Figures 4-7 are shown in appendix 1 for Mathematica and Matlab.

To eliminate numerical instabilities, the absolute error tolerance and the relative error tolerance were both set to 10^{-7} for Matlab. The mathematica graphs use the default tolerances. We note that Mathematica and Matlab were consistent with each other.

The constants k_1 and k_2 were picked arbitrarily. However, we know that k_1 is several orders of magnitude smaller than k_2 because the torsional torque is much smaller than the lever torque. The values of the constants we used in the numerical calculations are shown in Table 1. The results of the numerical calculations are shown in Figures 4-8.

Notice that $\phi(t)$ is not affected by the motion of $\theta(t)$, because Equation 22a does not depend on $\theta(t)$. Thus, the results shown in Figure 4 are harmonic. However, $\theta(t)$ depends on the value of $\phi(t)$. Figure 5 shows the results of our calculations for $\theta(t)$. The motion of θ is visually smooth and continuous, and seems sinusoidal. Closer examination reveals that is not exactly harmonic. This anharmonic property can be seen more clearly by examining the first and second derivatives of $\theta(t)$ which are shown in Figures 6 and 7. Notice that θ' and θ'' show anharmonic characteristics overlaid on a general harmonic shape. The reason for this is that the coupled motion of ϕ and θ. The anharmonic oscillations are caused by the non-constant term in front of θ in Equation 22b. This varies the amount of torque, changing the shape of $\theta(t)$ from being harmonic. The variation is small because of the choice of values of k_1 and k_2. The dotted line in Figure 7, the graph of $\theta''(t)$, is the graph of the simplified solution presented by Equation 24.

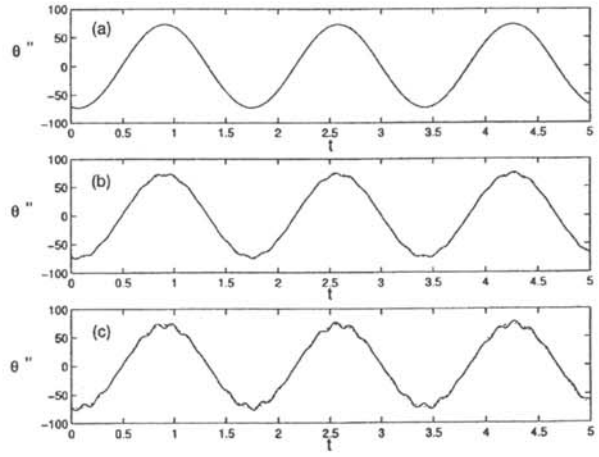

Figure 8
Multiple plots of θ″ versus t for several values of initial θ′ (a) θ′(0) = 0; (b) θ′(0) = 3; (c) θ′(0) = 6.

Our experience with the k_1 and k_2 parameters is that their different values affect not only the period of their associated motions, but also the anharmonic terms. By decreasing k_1, the anharmonic terms seem to increase. This is similar to what happens in Figure 8, which will be discussed later, but for a different reason.

In Figures 5 and 6, the only qualitative difference between the numerical solutions and the simplified analytical solution is the change in the period of the oscillations. The difference is, however, not discernible from the figures. The anharmonic motion of $\theta(t)$ can be eliminated by changing the initial angular velocity of $\phi(t)$. If $\phi'(0) = 0$, then $\phi(t)$ is a constant, and as in the simplified case, the anharmonic components disappear and $\theta(t)$ becomes harmonic. When the initial angular velocity of ϕ is increased, the variations of $\phi(t)$ increase and the motion of $\theta(t)$ becomes more anharmonic. This is illustrated in Figure 8.

ACKNOWLEDGMENTS

The author wishes to thank Dr. J.E. Hasbun for his guidance on this project. He also wishes to thank Dr. Scott Gordon for help with solving the differential equations.

REFERENCES

†. Current address of author: home: 1801 Inlet Lake Place, Snelville, GA 30078; School: PO Box 10298, Carrollton, GA 30118.
1. J.B. Marion, Classical Dynamics of Particles and Systems, Academic Press:New York, NY, (1965), Chapter 13.
2. H. Goldstein, Classical Mechanics, Addison-Wesley Publishing Company: Reading, MA, (1959), Chapter 4.
3. D. Halliday, R Resnick, and J. Walker, Fundamentals of Physics, John Wiley &Sons: New York, NY, (2001).
4. Mathematica 4.0, Wolfram research, http://www.wolfram.com. (1999).
5. Matlab 6.0, Mathworks, http://www.mathworks.com (20010.
6. Cosmic Ring Kinetic Mobile (item #79360), National Geographic Store, http://shop.nationalgeographic.com, April 12 2002.

FACULTY SPONSOR

Dr. J.E. Hasbun
Department of Physics
1600 Maple Street
State University of West Georgia
Carrollton, GA 30118
jhasbun@Westga.edu

APPENDIX 1

This appendix contains the specific commands used in the numerical computation of the solutions to Equations 22 with the parameters given in Table 1.

A) The Mathematica Program listing follows. For simplicity, we have employed the following changes of variables: t -> x, ϕ -> y, and θ -> z.

```
m=.05; h=.005; r2=.05; r1=.0495; k1=.0001; k2=.03;
Ixx = m*(1/3*h^2+1/4*(r2^2+r1^2));
Iyy = m*(1/3*h^2+1/4*(r2^2+r1^2));
Izz =1/2*m*(r2^2+r1^2);
k3 = (k1/4*(3/Ixx)+1/Izz))^(.5);
zprime0 = 3; yprime0 = 2; y0 = Pi/3; z0 = 5;
solution=NDSolve[{y''[x] == -k2/Iyy*(y[x]-Pi/3),
z''[x] == -k1((1/Ixx -1/Izz)*Sin[y[x]]^2+1/Izz)*z[x],
y[0] == 0, y' [0] == yprime0,  z[0] == 0,
z'[0] == zprime0}, {z,y}, {x,0,100}, MaxSteps->50000,
Method -> RungeKutta]
simplified[x_] := yprime0/k3*Sin[k3*x] + z0*Cos[k3*x]

Plot[{Evaluate[y[x] /.solution]}, {x, 0, 1}]
Plot[Evaluate[z[x]] /.solution], {x, 0.1, 5},

PlotStyle -> {{RGBColor[0, 0, 0]}, RGBColor[0, 0, 1],
Dashing[{0.01, 0.005}]}]

Plot[Evaluate[z''[x]] /.solution, simplified''[x]},
{x, 0.01, 5}]
PlotStyle -> {{RGBColor[0, 0, 0]},RGBColor[0, 0, 1],
Dashing[{0.01, 0.005}]}]
```

B) The Matlab Program listing "kmprojPAPER.m" folows below. Note that the separate function kmprojfuncdtion.m is also included.

```
%kmprojPAPER.m
%Set the parameter values
m=.05; h=.005; r2=.05'r1=.0495; k1=.001; k2=.1;
Ixx=m*(1/3*h^2 + 1/4*(r2^2+r1^2));
Iyy=m*(1/3*h^2 + 1/4*(r2^2+r1^2));
Izz=m*1/2*(r2^2 + r1^2);
k3=(k1/4*(3/Ixx + 1/Izz))^.5;
```

```
%Set the initial conditions
xinit=[pi/3;5;2;3];

%Integrate the system of 0 to 5
ODEOaraneters=odeset('RelTol',1e-7, 'AbsTol', 1e-7);
[t,X]=ode45('kmprojfunction',[00 5],xinit,
ODEParameters,Ixx,Iyy,Izz,k1,k2);

%Plot theta(t)
figure;
Simplified=3/k3*sin(k3*t) + 5*cos(k3*t);
plot(t,X(:,1));
plot(t,Simplified,'r:');

%Plot theta'(t)
figure;
Simplified=3/k3*sin(k3*t) - 5*cos(k3*t);
plot(t,X(:,4));
plot(t,Simplified,'r:');

%Plot theta''(t) and the simplified theata''(t)
figure; hold on;
Simplified=-k3^2*(3/k3*sin(k3*t) + 5*cos(k3*t));
Actual=-k1*((1/Ixx-1/Izz)*sin(X(:,1)).^2)+1/Izz).*X(:,2);
plot(t,Actual));
plot(t,Simplified,'r:');

%Plot phi(t)
figure;
plot(t,(X:,2));

%kmprojfunction.m
function xp=f(t,x,y0,Ixx,Iyy,Izz,k1,k2)
xp=x;
y=x(1); z=x(2);
p=x(3); q=x(4);
xp(1)=p;
xp(2)=q;
xp(3)=-k2/Iyy*(y-pi/3);
xp(4)=-k1*((1/Ixx-1/Izz)*sin(y)^2)+1/Ixx)*z;
```

JURP goes on-line ... the end of production evolution.
Rexford E. Adelberger, Editor

The production of JURP has gone through many stages of evolution during the past 20 years. When, in 1981, the AIP executive board approved the founding of the Journal of Undergraduate Research in Physics as the Journal of the Society of Physics Students and its honor society Sigma Pi Sigma, a small grant was given to purchase an Apple II computer and an impact printer.

The original word processor used to format the articles is now an antique. It sits on a shelf to become part of a museum. It had no spell checker, no equation editor and no graphic capabilities, but could fit on two 5 inch floppy disks. The hard disk in the Apple was so small that you had to change floppies to store the articles. The graphics were all formatted by hand, using a drawing board and an ink pen. It was a good thing that the editor had taken mechanical drawing in high school. During this time, the editor learned how difficult it is to proof read your own work. Once the copy was thought to be in proper English, the text for the articles was printed out in 4.25 inch wide columns and pasted onto a large sheet of paper in two column format. The equations were entered using press-on letters, and the graphics pasted into their appropriate places. The large story boards were then photographed, etched and printed.

After the first 5 volumes were produced, the production equipment was upgraded to a MacIntosh computer. The what-you-see-is-what-you-get format of the new word processor that could handle text, graphics and equations in a somewhat seamless manner was exciting and fun to use. The editorial office also purchased its first scanner and laser printer. It was truly amazing to the editor that he could scan in figures, and then use graphics software to modify and clean up the images. The pages of the journal now could be printed in photo-ready format with no need to paste various pieces of the copy into a story board.

The subscription list consisted of about 200 libraries and various individual subscriptions. The subscription list was kept on the same computer that produced the copy. Individual address labels were printed, and with the help of the editor's wife, were placed on the individual copies, each copy was sealed with tape, and then taken to the bulk mail area of the college's mail room. A large mailing consisted of about 700 copies.

As the editor also a professor of physics in a small liberal arts college, he received support from the college in the production of the journal. The college handled all of the financial record keeping and provided some of the costs of maintaining the editorial office a Guilford. This meant that the editor had to learn something about accounting, so that he could figure out how to read the balance sheets, etc. It became clear to him that accountants have a language and mathematics all of their own.

The editorial office moved with the editor as he went on sabbatical. Early on, one volume was produced on an old all-in-one MacIntosh computer in the city of Starnberg, Germany. The editor would format the copy while overlooking the alps and the Starnberger See. A Guilford, physics student, Dail Rowe, acted as business manager and handled the mail correspondence that came from Germany and all other things. A second time, the copy was edited and produced in the town of Kula on the slopes of Haleakala overlooking the paradise known as Maui. Again a Guilford physics student, Ari Betof, acted as business manager and ran the office at Guiford College. This time, communications were easy as the internet was available and very fast.

In 1987, the Society of Physics Students decided to send all members of the society a printed copy of the Journal. The production runs went from a few hundred to a maximum of 8 thousand. The mailing lists could no longer be kept at Journal office at Guilford College and labels printed. A bulk mailing service was used to send out the copies. Still another new skill had to be learned.

Then, yet another learning opportunity occurred; the old word processor that the editor finally mastered, was no longer supported. He had to start looking at other software systems to produce the copy. After many frustrating attempts to use WORD and WordPerfect to format the Journal, the decision was made to adopt PageMaker as the word processor. There were a couple of interesting consequences of the adoption of this word processor. First, and perhaps the most important at the time, was that the copy could be sent electronically to the printer. There no longer was a need to produce a hard copy that had photographed so that the journal could be printed using the off-set method.

The second is that it became possible to easily produce a copy of the Journal in pdf format. This made it possible to place old copies of the Journal in pdf format on a web page. The web page of the Journal is maintained by the American Institute of Physics and can be found at: http://www.JURP.org

At this time, the journal is no longer sent to each member of the Society of Physics Students. The current issue is still produced in a hard copy format that is sent to libraries and those individuals who subscribe to it.

The production of JURP is a mirror of the upgrading of a physicist, from an experimentalist who interfaced computers into nuclear counting experiments to a semi-skilled desk top publisher. Now that the editor of JURP is approaching his dotage and retirement as a teacher, he is also looking forward to gaining a few hundred hours per year when someone else takes over JURP and moves it to the next level.

PREPARING A MANUSCRIPT FOR PUBLICATION

Rexford E. Adelberger, Editor

Perhaps the most important thing for you to keep in mind when you write a manuscript which you intend to submit for publication to the Journal of Undergraduate Research in Physics is that the audience that will be reading the paper is a junior or senior physics major. The readers are knowledgeable about physics, but unlike you, they have not spent as much time trying to understand the specific work that is being reported in your paper. They also can read English well, and expect the paper to be written by a colleague, not a robot or an 'all-knowing' computer. There is a big difference between the comments you write in the margin of your lab notebook, or what you might write in a technical brief, and what you should present in a paper for publication in a scientific journal.

There is a significant difference between a Journal article and keeping a journal. Your laboratory data book should be the journal of what you did. It contains all the data, what you did (even if it was an attempt that turned out to be wrong), as well as comments as to what you were thinking at that time. The Journal article is an discussion of how you would do the research without excursions along blind alleys and hours spent collecting data that were not consistent. The reader does not have to be able to completely reproduce the work from the Journal article. The reader should be able to understand the physics and techniques of what was done.

The general style of writing that should be followed when preparing a manuscript for publication in the Journal is different from what you would submit to your English literature professor as a critique of some other work. The narrative of the paper is intended to do three things: 1) present the background necessary for the reader to appreciate and understand the physics being reported in the paper; 2) discuss the details of what you did and the implications of your work; 3) lead the reader through the work in such a way that they must come to the same concluding points that you did. When finished with your paper, the reader should not have to go back and try to decide for themselves what you did. Your narrative should lead them through your work in an unambiguous manner, telling them what to see and understand in what you did. The interpretation of the data or calculations should be done by the writer, not the reader. The interpretation of your results is the most important part of the paper.

You should take care to make sure that the material is presented in a concise logical way. You should make sure that your sentences do not have too many dependent clauses. Overly complicated sentences make the logic of an argument difficult to follow. You should choose a paragraph structure that focuses the attention of the reader on the development of the ideas.

A format which often achieves these aims is suggested below:

ABSTRACT : An abstract is a self contained paragraph that concisely explains what you did and presents any interesting results you found. The abstract is often published separately from the body of the paper, so you cannot assume that the reader of the abstract also has a copy of the rest of the paper. You cannot refer to figures or data that are presented in the body of the paper.

How a person uses Journal articles to find out about new ideas in physics is often done in the following way. A computerized search, using key words in abstracts, is performed to find what work others have done in the area of interest. If the abstract seems to be about the question of interest, the body of the paper is tracked down and read. If the reader then wants to find out the finer details of how to reproduce the experiment or the derivation of some equation, the author of the paper is contacted for a personal in-depth conversation about the more subtle details.

INTRODUCTION: This is the section that sets the background for the important part of the paper. It is not just an abbreviated review of what you are going to discuss in detail later. This section of the narrative should present the necessary theoretical and experimental background such that a knowledgeable colleague, who might not be expert in the field, will be able to understand the data presentation and discussion of results. If you are going to use a particular theoretical model to extract some formation from your data, this model should be discussed in the introduction.

Where appropriate, factual information should be referenced using end-notes. When presenting background information, you can guide the reader to a detailed description of a particular item with the statement such as: *"A more detailed discussion of laminar flow can be found elsewhere [1]"*. If you know where there is a good discussion of some item, you don't have to repeat it, just guide the reader to the piece.

How one proceeds from this point depends upon whether the paper is about a theoretical study or is a report on an experiment. We will first suggest a format for papers about experimental investigations and then one that describes a theoretical derivation.

Experimental Investigations

THE EXPERIMENT: This section guides the reader through the techniques and apparatus used to generate the data. Schematic diagrams of equipment and circuits are often easier to understand than prose descriptions. A statement such as *"A schematic diagram of the circuit used to measure the stopping potential is shown in Figure 6"* is better than a long elegant set of words. It is not necessary to describe in words what is shown in a diagram, unless you feel that there is a very special part which should be pointed out to the reader. If special experimental techniques were developed as part of this work, they should be discussed here. You should separate the discussion of the equipment used to measure something from your results. This section should not include data presentations or discussions of error analysis.

DATA PRESENTATION AND INTERPRETATION OF RESULTS: This is the most important section of the paper. The data are the truths of your work. This section should lead the reader through the data and how uncertainties were measured or assigned. Experimental values without accompanying uncertainties are meaningless. The numerical data values are presented in tables and figures, each with its own number and caption, e.g.. *"The results of the conductivity measurements are shown in Table 3"*. It is difficult to follow narratives where the numerical results are included as part of the narrative. Raw, unanalyzed data should not be presented in the paper. All figures and tables should be referred to by their number. Any figure or table that is not discussed in the narrative should be eliminated. Items which are not discussed have no place in a paper.

A Theoretical Study

THE MODEL: This part should consist of a theoretical development of the constructs used to model the physical system under investigation. Formulae should be on separate lines and

numbered consecutively. The letters or symbols used in the equations should be identified in the narrative, e.g.. *The potential can be approximated as:*

$$W \approx Z - \sigma(\rho) \ , \qquad (1)$$

where Z is the number of protons and σ is the screening constant that is dependent on the charge density, ρ, of the inner electrons of the K and L shells. If you wish to use this formula at a later time in the narrative, you refer to it by its number, e.g.. *"The straight line fit shown in Figure 3 means that we can use Equation 1 to extract a value of..."*

CALCULATIONS: This section presents a summary and discussion of the numerical results calculated from the model. The results should be presented in tables or graphs, each with a caption. A table or graph that is not discussed in the narrative should be eliminated. Data that are not interpreted by the writer have no place in a paper. One should reference numerical results that are used in the calculations and come from previous work done by others .

The following sections pertain to both types of papers.

CONCLUSIONS: It is indeed rare that one can come to clear and meaningful conclusions in one paper. I do not know of many papers where this section should be included.

REFERENCES: All references, numbered in order from beginning to end of the paper, are collected together at the end of the paper. You should be aware of the following format:

If the reference is a text-

1. A.J. Smith and Q.C.S. Smythe, Electromagnetic Theory, Addison Wesley, New York, (1962), p. 168.

If the reference is a journal-

2. J. Boswain, Journal of Results, 92, (1968), pp. 122-127.

If the reference is unpublished-

3) R.J. Ralson, private communication.

ACKNOWLEDGMENTS: This short section should acknowledge the help received (that is not referenced in the previous section) from others. This is where you would give credit to a lab partner or someone in the machine shop who helped you build a piece of equipment.

OTHER ADVICE

TABLES AND FIGURES are placed by the layout editors at the corners of the page to make the format attractive and easy to read. Often a figure is not on the same page as the discussion of the figure. Each table or figure should be numbered and have a caption which explains the figure. Readers scan papers by looking at the figures and data tables before they read the narrative of the work. Take care to put enough information in the caption of a figure or table so that the reader can get some feeling for the meaning of the data presentation. All lines shown on graphs should be identified, e.g.. *"The dashed line is drawn to guide the eye"* or *"The solid line is a fit to the data using the Ising model"*

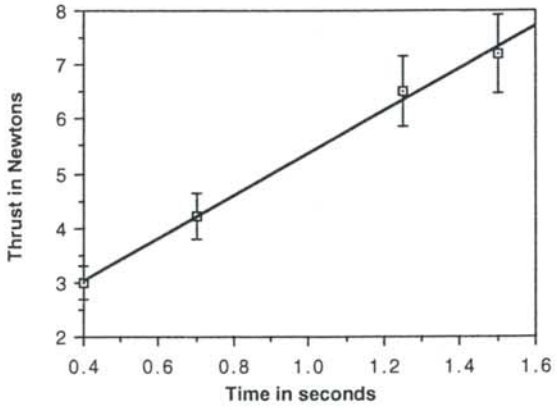

Figure 1

A graph of the measured thrust of a D-2 model rocket engine as a function of time. The line drawn is the least squares fit straight line to the data.

State	Experimental eV	Theoretical eV
3S	5.15±.01	5.13
4S	1.89±.02	1.93
3P	2.96±.02	3.02

Table 1

Energy states found in the numerical search. The accepted values for these states are also listed.

An example of a graph of a set of data is shown in Figure 1. The graph is sized by the range of data points. The bottom left point does not have to be the point (0,0). Error bars are shown with the data points. A graph with all the data points clustered in one small corner and lots of white space does not help the reader get a feeling of the dependence of your data. Be careful that the figures you present are not too busy; too much information on a figure makes it difficult to pick out the important parts.

NUMBERS AND UNITS Any experimentally measured data presented in tables (such as shown in Table 1), should include an uncertainty. You should use scientific notation when presenting numbers, $(7.34 \pm .03) \times 10^7$ eV. Take care that you have the correct number of significant digits in your results; just because the computer prints out 6 digits does not mean that they are significant. You should use the MKS system of units.

STYLE It is often helpful to make a flow chart of your paper before you write it. In this way, you can be sure that the logical development of your presentation does not resemble two octopuses fighting, but that it is linear.

One generally writes the report in the past tense. You already did the experiment. You also should use the third person neuter case. Even though you might have done the work by yourself, you use "we". e.g.. *"We calculated the transition probability for..."* It is often confusing when you begin sentences with conjunctions. Make sure that each sentence is a clear positive statement rather than an apology.

There are a few words or phrases you should be careful of using. ***Fact*** - this is a legal word. I am not sure what it means in physics. ***Proof or prove*** - These words are meaningful in mathematics, but you can't prove something in physics, especially experimental physics. ***The purpose of this experiment is...*** Often it is necessary to do the experiment to complete the requirements for your degree. You do not need to discuss the purposes of the experiment. ***One can easily show that...*** - Don't try to intimidate the reader. What if the reader finds it difficult to show? Remember that the reader of your paper is a senior in college! ***It is obvious that... or One clearly can see....*** - Such statements only intimidate the reader that does not find your work trivial. What is obvious to someone who has spent a lot of time thinking about it, may not be obvious to the reader of your paper. ***Data*** is the plural form of the noun datum. *"The data are ..."* or *"The data show that ...."*

The Journal of Undergraduate Research in Physics

The Journal of Undergraduate Research in Physics is the journal of Sigma Pi Sigma and the Society of Physics Students. It is published by the Physics Department of Guilford College, Greensboro NC 27410. Inquiries about the journal should be sent to the editorial office.

The Journal of Undergraduate Research in Physics ISSN 0731-3764

Editorial Office -
The Journal of Undergraduate Research in Physics
Physics Department
Guilford College
Greensboro, NC 27410
336-316-2279 (voice)
336-316-2951 (FAX)

Editor -
Dr. Rexford E. Adelberger
Professor of Physics
Physics Department, Guilford College
Greensboro, NC 27410
RAdelber@Guilford.Edu

Web Page -
http://www.jurp.org

The Society of Physics Students

National Office -
Dr. Gary White, Director
Ms. Sonja Lopez, SPS Supervisor
Society of Physics Students
American Institute of Physics
1 Physics Ellipse
College Park, MD 20740
301-209-3007

President of the Society -
Dr. Karen Williams
Department of Physics
East Central University, Ada, OK

President of Sigma Pi Sigma -
Dr. Steve Feller
Department of Physics
Coe College, Cedar Rapids, IA

- EDITORIAL BOARD -

tear along dashed line